The Canadian Mineralogist
Vol. 46, pp. 1555-1575 (2008)
DOI: 10.3749/canmin.46.6.1555

THE CRYSTAL CHEMISTRY OF THE SCAPOLITE-GROUP MINERALS. II. THE ORIGIN OF THE *I*4/*m* ⇄ *P*4$_2$/*n* PHASE TRANSITION AND THE NONLINEAR VARIATIONS IN CHEMICAL COMPOSITION

FRANK C. HAWTHORNE[§] AND ELENA SOKOLOVA

Department of Geological Sciences, University of Manitoba, Winnipeg, Manitoba R3T 2N2, Canada

ABSTRACT

The scapolite structure consists of two interpenetrating frameworks: $[(Si,Al)_{12}O_{24}]$ and $\{Na,Ca\}\{Cl,(CO_3)\}$. The unstrained dimensions of each framework are significantly different (as determined by the valence-matching principle and distance-least-squares refinement); there is an intrinsic steric stress between the two frameworks, the magnitude of which is a function of chemical composition. Evidence of the resulting structural strain is the large U_{eq} values for Cl at the *A* site across the marialite–meionite series and the large U_{eq} values for (Na,Ca) at the *M* site in marialite. Local bond-valence considerations indicate extensive SRO (Short-Range Order) about both Cl and (CO_3). The short-range bond-valence requirements of the (CO_3) group are satisfied by coordination with Ca_4 at ~Me_{100}, $NaCa_3$ at ~Me_{80}, Na_2Ca_2 at ~Me_{55}, Na_3Ca at ~Me_{40}, and Na_4 at ~Me_{20}. The driving mechanism for the *I*4/*m* ⟶ *P*4$_2$/*n* phase-transitions is the coupling of SRO between the $[(Si,Al)_{12}O_{24}]$ and $\{Na,Ca\}\{Cl,(CO_3)\}$ frameworks. At a composition of ~Me_{50}, local bond-valence requirements force the local clusters Na_2Ca_2 to occur in a *trans* configuration {NaCaNaCa} around the *A* site. Anion bond-valence requirements also force these clusters to link to each other through Na–O–Na or Ca–O–Ca linkages, and hence the combination of SRO and bond-valence requirements gives rise to LRO (long-range order). In turn, Al and Si are constrained to order at different tetrahedra, an ordering that breaks the topological *I*4/*m* symmetry and gives rise to two distinct tetrahedra, *T*(2) and *T*(3), dominated by Al and Si, respectively. The result is the *P*4$_2$/*n* scapolite structure. As Na or Ca become dominant, the number of Na_2Ca_2 clusters decreases, the effectiveness of the symmetry-lowering mechanism lessens, and the degree of order of Al and Si over the *T*(2) and *T*(3) sites decreases toward both the marialite and meionite ends of the series. At the compositions ~Me_{22} and Me_{78}, the clusters $NaCa_3$ and Na_3Ca dominate, the driving mechanism for lower symmetry vanishes, and the structures revert to maximal *I*4/*m* symmetry. The nonlinear variations in bulk composition across the marialite–meionite series are also the result of SRO of *M*-site Na and Ca around the *A* site [which is occupied by Cl in end-member marialite and (CO_3) in end-member meionite]. Local bond-valence requirements indicate extensive SRO about both Cl and (CO_3) in scapolite. In particular, Cl cannot occur in *I*4/*m* meionite except where K is present; in this case, chemical variations indicate that Cl enters the *I*4/*m* meionite structure as $\{ClK_2Ca_2\}$ clusters.

Keywords: scapolite, marialite, meionite, silvialite, end members, chemical composition, short-range order, phase transition.

SOMMAIRE

La structure des minéraux du groupe de la scapolite contiennent deux trames interpénétrantes: $[(Si,Al)_{12}O_{24}]$ et $\{Na,Ca\}\{Cl,(CO_3)\}$. Les dimensions sans contraintes de chaque trame diffèrent de façon importante, comme l'indiquent le principe de la corcordance des valences et un affinement par distance-moindres-carrés; il existe donc de façon intrinsèque des contraintes stériques entre ces deux trames, dont l'importance dépend de la composition chimique. Les valeurs élevées de U_{eq} des atomes Cl occupant le site *A* sur toute la série marialite–méionite, et de (Na, Ca) occupant le site *M* dans la marialite, témoignent de ces déformations structurales. Les considérations des valences de liaison indiquent l'importance de mise en ordre à courte échelle impliquant Cl et (CO_3). Les exigeances des valences de liaison du groupe (CO_3) à courte échelle seraient satisfaites par une coordinence avec Ca_4 à ~Me_{100}, $NaCa_3$ à ~Me_{80}, Na_2Ca_2 à ~Me_{55}, Na_3Ca à ~Me_{40}, et Na_4 à ~Me_{20}. Le mécanisme qui cause la transition de phase *I*4/*m* ⟶ *P*4$_2$/*n* est le couplage des mises en ordre à courte échelle entre les deux trames, $[(Si,Al)_{12}O_{24}]$ et $\{Na,Ca\}\{Cl,(CO_3)\}$. A une composition de ~Me_{50}, les exigeances locales des valences de liaison forcent les groupements locaux Na_2Ca_2 d'adopter une configuration *trans* {NaCaNaCa} autour du site *A*. Les exigeances des valences de liaison autour des anions de même forcent ces groupements d'atomes de s'agencer l'un à l'autre par des liaisons Na–O–Na ou Ca–O–Ca, de sorte qu'une combinaison des effets de mise en ordre à courte échelle et des exigeances des valences de liaison mène à une mise en ordre à longue échelle. A leur tour, les atomes Al et Si sont forcés d'occuper des tétraèdres différents, ce qui brise la symétrie topologique *I*4/*m* et donne lieu à deux tétraèdres distincts, *T*(2) et *T*(3), dans lesquels prédominent Al et Si, respectivement. Il en résulte la structure de symétrie *P*4$_2$/*n*. A mesure que Na ou Ca devient prédominant, le nombre de groupes Na_2Ca_2 diminue, le mécanisme

§ *E-mail address*: frank_hawthorne@umanitoba.ca

servant à diminuer la symétrie devient moins efficace, et le degré d'ordre de Al et Si sur les sites *T*(2) et *T*(3) diminue en direction des deux pôles de la série, marialite et méionite. Aux compositions ~Me_{22} et Me_{78}, les groupements $NaCa_3$ et Na_3Ca prédominent, le mécanisme servant à diminuer la symétrie disparait, et les structures adoptent leur symétrie maximale, *I*4/*m*. Les variations non linéaires des compositions globales dans la série marialite–méionite series résulteraient aussi de la mise en ordre à courte échelle des occupants Na et Ca du site *M* autour du site *A* [occupé par le Cl dans le pôle marialite et (CO_3) dans le pôle méionite]. Les exigeances des valences de liaison mènent à une importante mise en ordre locale autour des atomes Cl ainsi que des groupes (CO_3) dans la scapolite. En particulier, le Cl ne peut pas être accommodé dans la méionite *I*4/*m* sauf si le K est présent; dans ce cas, les variations chimiques indiquent que le Cl y est accommodé sous forme de groupements {ClK_2Ca_2}.

(Traduit par la Rédaction)

Mots-clés: scapolite, marialite, méionite, silvialite, end members, chemical composition, short-range order, phase transition.

Introduction

Sokolova & Hawthorne (2008) have presented detailed information on the crystal structures, chemical compositions and site populations across the marialite, $Na_4[Al_3Si_9O_{24}]Cl$, – meionite, $Ca_4[Al_6Si_6O_{24}]\{CO_3\}$, join of the scapolite-group minerals. Re-examination of the crystal chemistry of scapolite seems timely. In particular, there are several rather difficult issues associated with the marialite–meionite solid-solution series, and it is useful to identify them specifically here (not necessarily in order of importance):

(1) Why is there a nonlinear variation in chemical composition across the series? Although there is a general consensus that this nonlinear variation is the result of SRO of (Na,Ca) and {Cl,(CO_3)}, a quantitative understanding has not been developed.

(2) Why does the scapolite structure adopt *I*4/*m* symmetry close to both end-member compositions and $P4_2/n$ symmetry for intermediate compositions?

(3) Why is Al so strongly ordered over *T*(2) and *T*(3) in $P4_2/n$ structures of intermediate composition?

Figure 1 shows important components of the scapolite structure that will be referred to extensively in the following discussion.

Previous Work

Chemical composition

Shaw (1960a,b) reviewed the mineralogy, petrology and general geochemistry of the scapolite-group minerals. He discussed the difficulties in obtaining a pure mineral separate for chemical analysis, and rejected ~50% of the chemical compositions then available in the literature as unreliable. Evans *et al.* (1969) circumvented the purity issue that plagued previous analytical work by using an electron microprobe, and showed that the marialite–meionite join cannot be considered as a simple binary solid-solution. This general conclusion has been supported by all subsequent work (*e.g.*, Chamberlain *et al.* 1985, Teertstra & Sherriff 1996, Zolotarev 1996, Seto *et al.* 2004). However, the details of the non-binary chemical behavior in this series are still not completely clear. Evans *et al.* (1969) proposed that there are two distinct series, $Me_{0–75}$ and $Me_{75–100}$, and this view was supported by Ulbrich (1973), Aitken *et al.* (1984) and Hassan & Buseck (1988). Zolotarev (1996), Zolotarev *et al.* (2003) and Teertstra & Sherriff (1996, 1997) proposed that there are three distinct series, $Me_{0–24}$, $Me_{24–64}$ and $Me_{64–100}$, and 9.0 > Si > 8.4, 8.4 > Si > 7.3 and 6.3 > Si > 6.0 *apfu* (atoms per formula unit). Seto *et al.* (2004) showed that a large range of compositions adhere more closely to the trends proposed by Zolotarev (1996) and Sherriff & Teertstra (1996, 1997) than to the trend proposed by Evans *et al.* (1969).

Symmetry

The structure of scapolite was solved in the space group *I*4/*m* (Gossner & Brükkl 1928, Pauling 1930, Schiebold & Seumel 1932). Later investigators (Papike & Zoltai 1965, Papike & Stephenson 1966) also refined the structure of scapolites in *I*4/*m*, but noted the presence of weak reflections violating the *I*-centering (*i.e.*, $h + k + l = 2n + 1$). Lin & Burley (1973a, b, 1975) showed that scapolite close to end-member compositions has space-group symmetry *I*4/*m*, whereas intermediate compositions have space-group symmetry $P4_2/n$. All subsequent single-crystal X-ray-diffraction studies (Peterson *et al.* 1979, Aitken *et al.* 1984, Comodi *et al.* 1990, Belokoneva *et al.* 1991, 1993) are in accord with these results. However, Phakey & Ghose (1972) reported space-group symmetry *P*4/*m* or *P*4 by electron diffraction, and also noted the presence of antiphase domains. High-resolution transmission-electron microscopy studies of scapolite by Buseck & Iijima (1974) and Hassan & Buseck (1988) are in accord with the occurrence of *P*4/*m* or *P*4 symmetry, whereas similar observations by Oterdoom & Wenk (1983) are not. Seto *et al.* (2004) examined 21 samples by electron diffraction and made extensive checks for multiple diffraction. Violations of $P4_2/n$ symmetry were shown to be due to multiple diffraction in all cases (except for one point on one sample); Seto *et al.* (2004) found that previous reports of lower symmetry are due to multiple diffraction. Furthermore, they reported that all crystals of meionite examined show reflections violating *I*-centering; even Me_{90} shows weak reflections with *h*

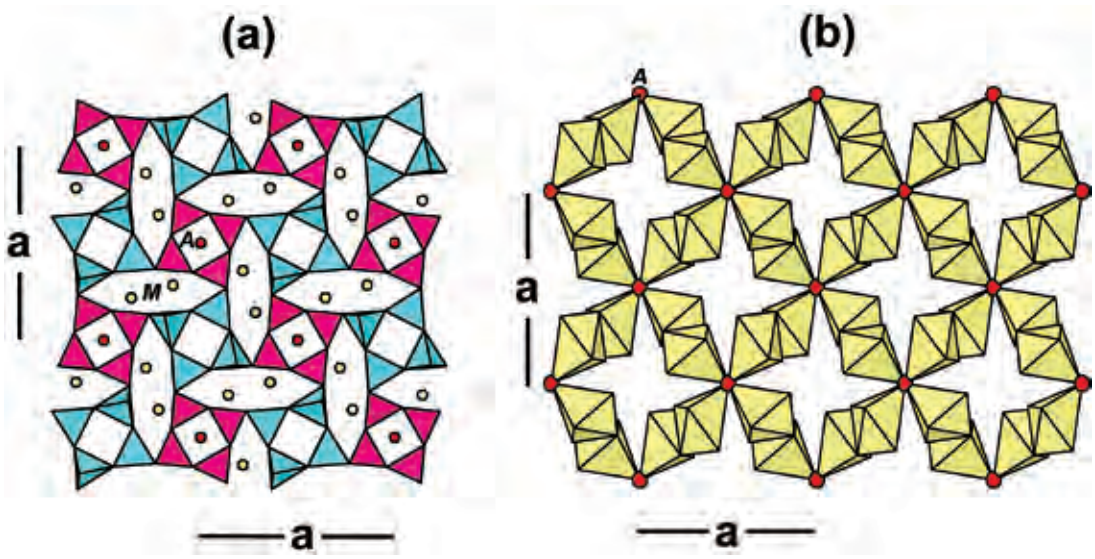

FIG. 1. The two frameworks in the crystal structure of *I*4/*m* scapolite projected along [001]: (a) the $[(Al,Si)_{12}O_{30}]$ framework; (b) the $[\{Na,Ca\}_4\{Cl,(CO_3)\}]$ framework. The *T*(1) tetrahedra are red, the *T*(2) tetrahedra are blue, the M polyhedra are yellow and the *A* site is shown as a red circle.

+ *k* + *l* = 2*n* + 1, whereas Na-rich marialite shows no such reflections.

Short-range order

Short-range order (SRO) describes the *local* association of species at neighboring (usually NNN, Next-Nearest Neighbor) sites in a structure. Some aspects of SRO have been addressed previously in the scapolite-group minerals. Work has focused on either (1) SRO involving Na, Ca, Cl and (CO_3) at or near the *A* sites within the cages of the aluminosilicate framework, or (2) Si–Al at the *T* sites of the aluminosilicate framework.

Chamberlain *et al*. (1985) examined possible local configurations involving Na, Ca, Cl and (CO_3) in scapolite of intermediate composition using calculations of the electrostatic energy. They calculated the structure energies for various configurations of these species and concluded that short-range order of Na_4Cl and $Ca_4(CO_3)$ occurs in intermediate scapolite and may give rise to antiphase domains. Hassan & Buseck (1988) argued that the observed variation in chemical composition across the marialite–meionite series indicates that local clusters of the types $\{Na_4Cl\}$ and $\{NaCa_3(CO_3)\}$ must occur in intermediate compositions [together with $\{Ca_4(CO_3)\}$ in meionite close to end-member composition]. Furthermore, Hassan & Buseck indicated that a model (for a crystal of composition $Me_{39.5}$) with clusters $\{Na_4Cl\}$ and $\{NaCa_3(CO_3)\}$ in the cages at (¼,¼,¼) and (¾,¾,¾), respectively, gave simulated images closer to the observed images than a "disordered model" (details not exactly specified but presumably consisting of partial atoms at the *M* sites and complete adherence to $P4_2/n$ symmetry). Their model for compositional variation within the marialite–meionite series is as follows: (1) $Me_{0–75}$: $\{Na_4Cl\}$ Si ⇄ $\{NaCa_3(CO_3)\}$ Al; (2) $Me_{75–100}$: $\{NaCa_3(CO_3)\}$ Si ⇄ $\{Ca_4(CO_3)\}$ Al.

Sokolova *et al*. (1996) and Sherriff *et al*. (1998, 2000) examined aspects of Al–Si order in both *I*4/*m* and $P4_2/n$ scapolite using ^{27}Al and ^{29}Si MAS NMR spectroscopy. Sokolova *et al*. (1996) showed that, in *I*4/*m* marialite, up to 80% of the Al atoms at the *T*(2) site are involved in the local configuration Al–O–Al. In *I*4/*m* meionite, Sherriff *et al*. (2000) proposed that there are Al–O–Al linkages between the *T*(1) and *T*(2) sites. In intermediate $P4_2/n$ compositions, Sherriff *et al*. (1998) proposed that the structure is "well-ordered" where Al = 4 *apfu*, and that Al–Si disorder and Al–O–Al configurations occur for Al < 4 *apfu* and Al > 4 *apfu*.

STRUCTURAL STRAIN

In dealing with solid solutions and phase transitions, structural strain is a significant issue. Structural strain may be caused by several factors; of particular interest here are (1) strain due to possible intrinsic deviations from the valence-sum rule of bond-valence theory (*i.e.*, deviations that arise from the bond topology and the valence states of the cations and anions), and (2) strain due to the dimensional misfit of linked structural components. With regard to (1), Brown (2002) has discussed

the methods for calculation of ideal bond-valences in structures. Specifically, one uses the equations involved in the valence-sum rule together with the equations of the equal-valence rule (Brown 2002), and solves for the unknown bond-valences. The equations involved in the valence-sum rule may be written as follows:

$$\sum_{j=1\rightarrow n} s_{ij} = V_i \text{ for cations, } i = 1 \rightarrow m$$
$$\sum_{i=1\rightarrow m} s_{ij} = V_j \text{ for anions, } j = 1 \rightarrow n \quad (1)$$

where s_{ij} is the bond valence between the i^{th} cation and the j^{th} anion, V_i and V_j are the formal valences of the i^{th} cation and the j^{th} anion, and m_i and n_j are the coordination numbers of cations and anions, respectively. The equations of the equal-valence rule may be written as

$$\Sigma s_{ij} = 0 \quad (2)$$

where the summation is over the bond valences around any closed loop in the digraph of the bond network of the structure. For marialite, there are twelve crystallographically distinct bonds, and hence we require twelve distinct equations to solve for s_{ij}. There are three cation sites and five anion sites, and hence eight equations of type (1), of which only seven contribute to the solution, as the electroneutrality principle makes one of these equations redundant; the balance of the equations are made up of type (2). Solving these equations simultaneously gives the bond-valence structure shown in Table 1. It is immediately noticeable that the valence-sum rule is adhered to exactly, and hence there is no intrinsic strain associated with the bond topology of the *I*4/*m* marialite structure.

TABLE 1. BOND VALENCES IN THE IDEAL UNSTRAINED *I*4/*m* END-MEMBER MARIALITE (UPPER) AND MEIONITE (LOWER) STRUCTURES*

	T(1)	*T*(2)	*M*	Σ
O(1)	1.000 1.000			2.000
O(2)		0.925	0.150	2.000
O(3)		0.925 0.925	0.150	2.000
O(4)	1.000	0.850	0.075 0.075	2.000
Cl			0.250	1.000
Σ	4.000	3.625	1.000	
O(1)	1.000 1.000			2.000
O(2)		0.883	0.234	2.000
O(3)		0.883 0.883	0.234	2.000
O(4)	0.75	0.85	0.200 0.200	2.000
(CO_3)			0.500	2.000
Σ	3.500	3.500	2.000	

* the superscripts and arrows indicate bond multiplicities different from unity. Bond valences are expressed in valence units.

For meionite, the situation is more complicated owing to disorder of the (CO_3) group in the structure, and any calculation must involve some spatial averaging of at least part of the structure. Figure 2 shows a fragment of the meionite structure with an ordered (CO_3) group. It is apparent that the four Ca atoms linked to the (CO_3) group are not equivalent. Let us assume an average model for the (CO_3) group and the Ca–O bonds to the carbonate group, as this then allows solution of the relevant equations of types (1) and (2). The result (Table 1) adheres to the valence-sum rule exactly, and hence there is no long-range intrinsic strain associated with the bond topology of the *I*4/*m* meionite structure.

Dimensional Mismatch in the Structure of Scapolite

The scapolite structure consists of two elements, an $[(Al,Si)_{12}O_{24}]$ framework and an $\{Na,Ca\}_4\{Cl,(CO_3)\}$ framework (Sokolova & Hawthorne 2008).

The dimensions of the unstrained framework

A necessary but not sufficient condition for a structural arrangement to be unstrained is that the structure obey exactly the valence-matching principle (Brown 1981, Hawthorne 1994, 1997b). The bond-valence table for scapolite S(1) is shown as Table 2. Examination of the bond-valence sums indicates that the bond-valence sum incident at the *A* site is 0.57 *vu* (valence units), far less than the value of 1.00 *vu* required by the valence-sum rule. In order for the *A* site to conform to the valence-sum rule, the *M*–Cl bond must have a bond valence of 0.25 *vu*. According to the bond-valence curve for the Na–Cl bond (Brese & O'Keeffe 1991), 0.25 *vu* corresponds to a bond length of 2.663 Å. The structural arrangement that is conformable with this bond length may be calculated using the method of Distance Least-Squares (DLS, Meier & Villiger 1969, Baerlocher *et al.* 1977) applied to the $\{Na,Ca\}_4\{Cl,(CO_3)\}$ framework. The cell dimensions of the resulting structure are given in Table 3 (line 1). Similarly, we may calculate the unstrained cell dimensions for the $[(Al,Si)_{12}O_{30}]$ framework using ideal distances for the T(1) and T(2) tetrahedra. There are two ways in which we may define ideal distances for the *T*(1) and *T*(2) tetrahedra: (1) we may calculate the distances from the universal bond-valence curve of Brown (1981) for the isoelectronic series Na…P, which includes Al and Si; the resulting values are 1.622 Å for <*T*(1)–O> and 1.660 Å for <*T*(2)–O>;

(2) we may use <*T*–O> distances for the corresponding Al–Si occupancies from typical curves for framework aluminosilicates; the corresponding values are 1.605 Å for <*T*(1)–O> and 1.662 Å for <*T*(2)–O>. The resulting cell dimensions are given in Table 3. Although the adoption of different values for <*T*(1)–O> and <*T*(2)–O>, as indicated above, does produce different unit-cell dimensions, the results are similar in terms of the cell dimensions of the scapolite structure. The unstrained $\{Na,Ca\}_4\{Cl,(CO_3)\}$ framework is significantly smaller than the observed S(1) scapolite structure, whereas the unstrained $[(Al,Si)_{12}O_{30}]$ framework is larger than the observed S(1) scapolite structure. As noted above, these two frameworks interpenetrate, and hence their dimensions must be identical in the actual structure. However, the intrinsic (unstrained) dimensions of each framework are different, resulting in an intrinsic steric stress between the two frameworks.

We may do a similar calculation for crystal S(18). For the $\{Na,Ca\}_4\{Cl,(CO_3)\}$ framework, we may set the M–O(7,8,9) distances such that the (CO_3) group receives an aggregate incident bond-valence of 2 *vu*, in accord with the valence-matching principle. For the $[(Al,Si)_{12}O_{30}]$ framework, we set the <*T*–O> distances to appropriate values for the observed site-populations. The resulting values are given in Table 3. As for crystal S(1), the unstrained $[\{Na,Ca\}_4\{Cl,(CO_3)\}]$ framework is smaller than the observed S(18) scapolite structure, whereas the unstrained $[(Al,Si)_{12}O_{30}]$ framework is larger than both. However, the relative differences in the sizes of the unstrained frameworks is approximately twice as large in marialite S(1) as in meionite S(18). Hence the structural strain decreases across the series from marialite to meionite.

Direct evidence of structural strain

Can we see any direct experimental evidence of this dimensional mismatch? Examination of Table 5 of Sokolova & Hawthorne (2008) shows that the equivalent isotropic-displacement parameters of Cl at the *A* site are anomalously high, with an average value of 0.052 across the complete series. From crystals S(1) to S(8), the values are very tightly clustered about this mean value; in crystals S(9) to S(18), there is more scatter in the values, probably the result of the smaller amounts

TABLE 2. BOND-VALENCE TABLE* FOR SCAPOLITES
S(1) (TOP) AND S(18)** (BOTTOM)

	T(1)	*T*(2)	*M*	*C*	Σ
O(1)	1.063 1.052				2.115
O(2)		0.903 ×2 →	0.229		2.035
O(3)		0.927 0.912	0.160 ×2 ↓		1.999
O(4)	1.030 ×2 ↓	0.878	0.084 ×2 ↓ 0.079 ×2 ↓		2.071
Cl			0.142 ×4 →		0.568
Σ	4.175	3.62	1.017		
O(1)	0.979 0.964				1.943
O(2)		0.864 ×2 →	0.326		2.054
O(3)		0.856 0.856	0.234 ×2 ↓		1.946
O(4)	0.856 ×2 ↓	0.841	0.163 ×1 ↓ 0.106 ×2 ↓		1.966
O(7)			0.239 0.335	1.333	1.907
O(8)			0.124 0.445	1.333	1.902
O(9)			0.585 0.086	1.333	2.004
Σ	3.655	3.417	1.786	4	

* calculated with the curves of Brown (1981); bond valences are expressed in valence units.
** as the carbonate group is disordered with regard to the space-group symmetry of the crystal, the average interaction between *M* and the O anions of the carbonate group is the sum of all *M*–O (7,8,9) bond-valences divided by 4 (see Sokolova & Hawthorne 2008, Fig. 14).

TABLE 3. COMPARISON OF CALCULATED UNSTRAINED FRAMEWORK DIMENSIONS WITH OBSERVED UNIT-CELL DIMENSIONS IN SCAPOLITE STRUCTURES OF SIMILAR COMPOSITION

	S(1)			S(18)		
	a (Å)	*b* (Å)	*V* (Å^3)	*a* (Å)	*b* (Å)	*V* (Å^3)
$[\{Na,Ca\}_4\{Cl(CO_3)\}]$ framework	11.727	7.639	1050.6	12.049	7.656	1111.6
scapolite structure (observed)	12.057	7.564	1099.6	12.208	7.583	1130.2
$[(Al,Si)_{12}O_{24}]$ (1)*	12.115	7.665	1125.0	12.175	7.730	1145.9
$[(Al,Si)_{12}O_{24}]$ (2)*	12.058	7.664	1114.3	–	–	–

*(1) calculated using <*T*–O> distances from the universal bond-valence curves of Brown (1981);
(2) calculated using <*T*–O> distances from typical occupancy – bond-length relations for framework aluminosilicates.

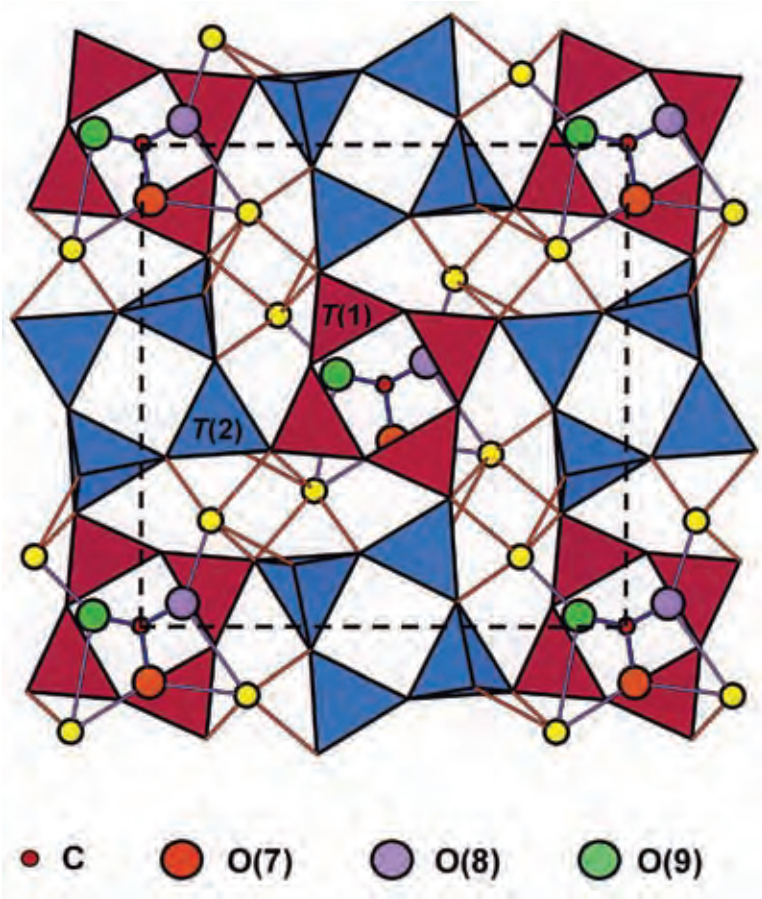

FIG. 2. The structure of *I*4/*m* meionite showing an ordered arrangement of (CO_3) groups and the coordination of their constituent oxygen anions by adjacent M cations.

of Cl and the increasing amounts of (CO_3) in these crystals. These high values of displacement suggest that Cl is displaced off the central (0, 0, ½) position in an attempt to attain a higher incident bond-valence sum by shortening one or more *M*–Cl bonds. Of course, such a displacement will lead to shortening of one or two bonds, but it will also produce a lengthening of the remaining bonds, producing only a small increase in the incident bond-valence. Another spontaneous displacement will occur in the opposite direction in an attempt to find a more optimal position, but this too will be unsuccessful. The high equivalent isotropic-displacement parameters for Cl are probably the result of dynamic displacement of Cl off the (0, 0, ½) position as a result of the dimensional misfit of the [{Na,Ca}$_4${Cl,(CO_3)}] and the [$(Al,Si)_{12}O_{30}$] frameworks.

The other component of the {Na,Ca}$_4${Cl,(CO_3)} framework is the *M* site. The long-range bond-valence sum at the *M* site as a function of bulk composition is in reasonable accord with the valence-sum rule, indicating that the majority of the strain in the {Na,Ca}$_4${Cl,(CO_3)} framework involves the *A* site. However, inspection of the equivalent isotropic-displacement parameters at the *M* site does show that they are anomalously high in marialite but are much lower in meionite (Fig. 3). The fact that the valence-sum rule is satisfied at the *M* site indicates that the unusually high equivalent isotropic-displacement parameters at the *M* site are not the direct result of the central cation displacing in order to satisfy its bond-valence requirements. However, in marialite, a significant amount of the incident bond-valence is supplied by Cl, which (we conjecture) is dynamically disordered about the *A* site. Although the static (which is equivalent to the time-averaged) arrangement obeys the valence-sum rule, the instantaneous arrangement does not, and the *M* cation will respond by dynamic displacement that is coupled to the movement of Cl about the *A* site. In meionite, the dominance of (CO_3)

dampens the effect, and Figure 3 shows that the equivalent isotropic-displacement parameter at the *M* site decreases with increasing (CO_3) content, in accord with this argument.

As we will see, this dimensional mismatch between the two frameworks of the scapolite structure is a major factor in the unusual nonlinear behavior of the marialite–meionite series.

Structural Strain and Its Expression in Terms of Bond Valence

When using bond-valence theory to consider aspects of crystal structures, we use the valence-sum principle of Brown (1981), which states that *the sum of the bond valences at an ion is approximately equal to the formal charge of that ion*. We have seen above that this rule is not necessarily true in all circumstances; where *A* = Cl in *I*-centered marialite, the sum of the incident bond-valence is 0.57 *vu*, far less than the formal valence of Cl^{1-}. In this case, we postulated that Cl is dynamically displaced off the central position to accommodate this situation. Other examples of significant deviation from the valence-matching principle are well known, *e.g.,* the low incident bond-valence sums at the O(2) anion in pyroxenes and the O(4) anion in amphiboles (Hawthorne 1983). These are examples of structural strain. The structure is obviously able to accommodate such strain (or the structure would not occur), and the apparently anomalous incident bond-valence sums are an expression of this strain. Such strains are related to the details of the coordination of cations and anions in the structure, *i.e.*, they are a function of the bond topology and chemical composition of the structure, and as such, they should vary systematically within a specific structure-type. As the bond topology is fixed for a specific structure-type, such strain should be a function of the variation in coordinating cations, *i.e.*, a function of the bulk composition of the crystal. Although we have noticed such systematic variations at the O(4) site in amphiboles, this aspect of structure has not been examined completely for a specific structure-type. Here, we do so for the scapolite structure. The scapolite structure is an ideal example in which to examine this issue: (1) it has two interpenetrating frameworks that must articulate across changing compositions of both frameworks; (2) it has fairly high symmetry, which constrains relaxation in response to chemical change; (3) it has two phase transitions that can be characterized in terms of strain.

The variation in incident bond-valence sums at the framework anions in the structure are shown as a function of composition in Figure 4. What is immediately apparent is that some anions in the structure deviate significantly from the valence-sum rule, exhibiting significant structural strain, and also that these deviations change systematically as a function of bulk composition of the structure. Several factors affect the structural arrangement: (1) the need to conform as closely as possible to the valence-sum rule, (2) the need to conform to the symmetry of the structure, (3) the need to respond to variations in temperature and

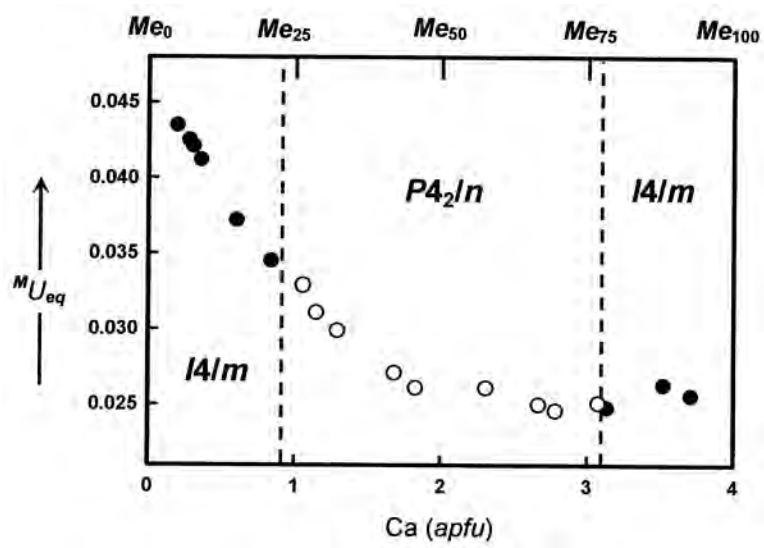

FIG. 3. Variation in the equivalent isotropic-displacement parameters of the *M* site as a function of Ca content; *I*4/*m* structures are shown in as black circles, $P4_2/n$ structures are shown as white circles.

pressure, (4) the need to respond to variations in bulk chemical composition. These factors are not necessarily completely compatible, and the observed structure will be a compromise among the optimal arrangements for each of these factors alone. As such, the observed *long-range* bond-valences will be a measure of the strain associated with this compromise. This leads us to a very important point with regard to *short-range* arrangements of atoms within the structure: rather than the sum of the incident bond-valences tending toward the formal valence of the ion, it seems more reasonable that *this sum tend toward the (observed) sum of the incident long-range bond-valences for the bulk composition under consideration.* In proposing a short-range equivalent to the valence-sum rule of Brown (1981), it seems reasonable to build into this rule a measure of the long-range strain such that the difference in strain between the *short-range* arrangement and the long-range structure is minimized, *i.e.*, the *local* strain associated with the short-range arrangement is at a minimum with respect to the long-range structure.

The $I4/m \rightleftarrows P4_2/n$ Phase Transitions

The results of Sokolova & Hawthorne (2008) suggest that the transition from the *I*4/*m* marialite structure to the $P4_2/n$ marialite structure is bounded by the compositions of crystals S(6) and S(7), *i.e.*, 0.848 < Ca < 1.055 *apfu*, and that the transition from the $P4_2/n$ meionite structure to the *I*4/*m* meionite structure is bounded by the compositions of crystals S(15) and S(16), *i.e.*, 3.082 < Ca < 3.119 *apfu*. The composition of the $I4/m \rightleftarrows P4_2/n$ marialite transition does not agree with that proposed by Seto *et al.* (2004): 0.691 < Ca < 0.714 *apfu*, involving a difference of ~0.249 Ca *apfu*. The composition of the $P4_2/n \rightleftarrows I4/m$ meionite transition does not agree with that proposed by Seto *et al.* (2004): 3.527 < Ca *apfu*, involving a difference of ~0.427 Ca *apfu*. However, the composition proposed by Teertstra & Sherriff (1997) for this transition is Ca ≈ 2.7 *apfu*, involving a difference of ~0.427 Ca *apfu* in the opposite sense: Seto *et al.* (2004) observed APDs (Anti-Phase Domains) in all samples of $P4_2/n$ scapolite

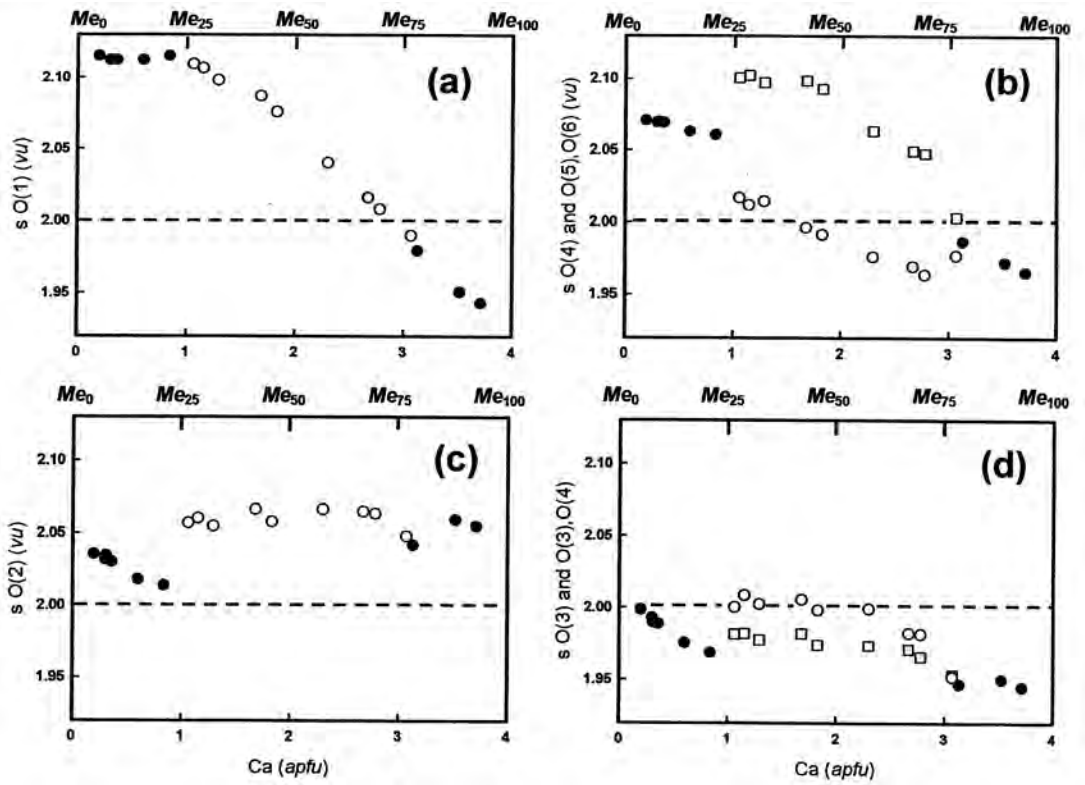

FIG. 4. Variation in the sums of the bond valences incident at (a) the O(1) anion; (b) the O(4) anion (*I*4/*m* structures) and O(5), O(6) anions [$P4_2/n$ structures; circles: O(5); squares: O(6)]; (c) the O(2) anion; (d) the O(3) anion (*I*4/*m* structures) and O(3), O(4) anions [$P4_2/n$ structures; circles: O(6); squares: O(5)] as a function of Ca content across the marialite–meionite series; *I*4/*m* structures are shown as black circles, $P4_2/n$ structures are shown as white symbols.

that they examined, indicating that $P4_2/n$ scapolite initially grew as $I4/m$ scapolite and inverted to $P4_2/n$ symmetry on cooling, and go on to suggest that $I4/m$ symmetry may persist metastably in the case of very rapid cooling.

We suggest the following explanation for the variation in transition composition reported by various authors, taking into account the observations of Seto *et al.* (2004) on the ubiquitous presence of APDs in $P4_2/n$ scapolite. The size of the APDs is likely to be a function of the rate of cooling of the crystal, smaller APDs being associated with rapidly cooled crystals. Very small APDs may not be registered by X-ray diffraction, whereas they may be registered by electron diffraction because the smaller wavelength of electrons relative to that of X-rays results in diffraction coherence from a smaller volume for electron diffraction than for X-ray diffraction. In addition, even if the size of APDs are large enough to allow diffraction of X-rays, aspects such as crystallinity and crystal size may also affect the observation of reflections incompatible with *I*-centered symmetry. The possible result is summarized in Figure 5. A composition [1] that crystallizes with $I4/m$ symmetry and cools very quickly may have APDs too small to give X-ray reflections that violate the condition $h + k + l = 2n$, and appear to have $I4/m$ symmetry at ambient temperature. On the other hand, a composition [2] that crystallizes with $I4/m$ symmetry and cools very slowly may have APDs sufficiently large to give to X-ray reflections that violate the condition $h + k + l = 2n$ and appear to have $P4_2/n$ symmetry at ambient temperature. Electron diffraction may indicate $P4_2/n$ symmetry for both compositions [1] and [2] under the cooling conditions specified. Thus the experiments on various samples with both X-ray and electron diffraction will give rise to an apparent range of compositions for the transition, as indicated schematically in Figure 5. We suggest that this is the case for the $I4/m \rightleftarrows P4_2/n$ phase transitions in the marialite–meionite series.

For purposes of discussion, we still need to specify (approximate) compositions at which changes in symmetry occur. We will use the values Me_{22} and Me_{78}, respectively.

The Marialite–Meionite Solid-Solution Revisited

As noted above, many investigators have emphasized that marialite–meionite is not a simple binary solid-solution. However, no consensus has yet emerged as to the exact nature of this variation, or the factors affecting the nonlinear variation in chemical composition from marialite to meionite. The data of Evans *et al.* (1969, Figs. 4, 5) show only a small amount of scatter about their general trends, a result that they assign to the high analytical precision of their electron-microprobe data. Teertstra & Sherriff (1997) re-analyzed many samples reported in the literature, and comparison of the two sets of results (Teertstra & Sherriff 1997, Fig. 9) show significant differences. On the other hand, Zolotarev (1996) and Zolotarev *et al.* (2003) compiled data from the literature, and these data show considerable scatter about the general trends. Comparison of these three sets of results suggests that much of the scatter of the data about the general trends may be due to analytical error. In this regard, the data of Sokolova & Hawthorne (2008) show very little scatter about the general trend. However, is all of the scatter about the general trend in the data for scapolite reported in the literature due to analytical error or is there some effect of conditions of crystallization? Seto *et al.* (2004) showed that zoned crystals of scapolite can show various compositional trends, all of which are inclined at a fairly shallow angle to the marialite–meionite join, and they proposed that these different compositional trends are caused by different P–T conditions of crystallization. Kullerud & Erambert (1999) reported compositional variations in scapolite crystallized at high pressure (8–11 kbar, 550–620°C), and Rebbert & Rice (1997) reported scapolite compositions crystallized at lower pressure (3.5–6 kbar, 450–670°C). Seto *et al.* (2004) noted that these results are not conformable with the compositional variation in some of their own samples, and suggested that other variables also affect such variations. However, in terms of the oscillatory-zoned scapolite crystals reported by Seto *et al.* (2004),

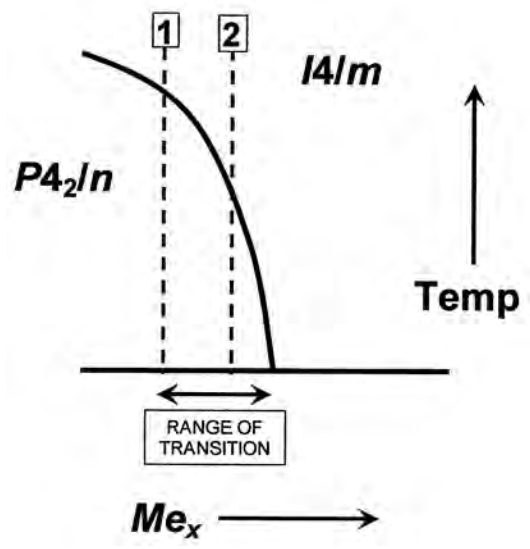

FIG. 5. Sketch of the possible behavior of meionite at the $I4/m \rightarrow P4_2/n$ transition; composition 1 is cooled rapidly, resulting in very small antiphase domains (or even quenching of the $I4/m$ structure), and $I4/m$ symmetry is indicated by X-ray diffraction; composition 2 is cooled slowly, resulting in large antiphase domains, and $P4_2/n$ symmetry is indicated by X-ray diffraction.

they did not consider the possibility that these oscillatory patterns arose *via* coupled feedback mechanisms involving differential diffusion. The general issue of what factors affect the chemical composition of scapolite is not yet clear.

End-member compositions

Although the non-binary nature of the scapolite (marialite–meionite) solid-solution has been emphasized in many studies, all end members of this series have not been explicitly identified. Of course, where these end members are valid mineral species, *e.g.*, marialite, meionite, silvialite, they are well known. However, where they do not occur in sufficient amounts to be the dominant component, they have not been considered. The additional end-members (components) are as follows: [0] $Na_4[Al_2Si_{10}O_{24}](CO_3)$ and [7] $Ca_4[Al_7Si_5O_{24}]Cl$, where the numbers in square brackets are used to identify these specific compositions in Table 4; note that these compositions are conformable with the criteria for an end member given by Hawthorne (2002). Thus (sulfate-free) scapolite can be represented in terms of the four end-members [0], [1] $Na_4[Al_3Si_9O_{24}]Cl$, [6] $Ca_4[Al_6Si_6O_{24}](CO_3)$ and [7] (Table 4). Because of compositional degeneracy, any specific composition needs only a maximum of three end-members to describe its composition, but the complete series requires all four end-members.

Variation in chemical composition

Compositional variation for the scapolite structure may be graphically represented in the system A–M–T, where A is the (CO_3) content [$(CO_3) \rightleftarrows Cl$], M is the Ca (Ca = Ca + Sr + Fe^{2+}) content (Ca $\rightleftarrows$ Na), and T is the Al content (Al $\rightleftarrows$ Si) (Fig. 6a). Table 4 lists the end-member compositions (shown by numbers in square brackets) and other compositions of interest (shown by numbers in parentheses). All compositions in Table 4 are coplanar in Figure 6a, and the broken line joins the end-member compositions of marialite, [1], and meionite, [6]. The shaded plane in Figure 6a shows the range of scapolite compositions algebraically possible for the scapolite structure, that is with the stoichiometry of the structural formula and obeying the electroneutrality principle. Seto *et al.* (2004) showed a large number of compositions of scapolite projected onto a version of this plane (but with non-orthogonal axes, *i.e.*, the vectors [1] → (2) and [1] → (5) defining their coordinate system are geometrically orthogonal but not algebraically orthogonal, see Fig. 6a). Their plot shows that all data scatter non-randomly about the marialite–meionite join, with large areas of the plane void of data. It is thus apparent that there are major crystal–chemical constraints on the possible compositions adopted by the scapolite structure (otherwise, the data points would cover the whole plane). Comparison of the data of Sokolova & Hawthorne (2008) projected onto the shaded plane of Figure 6a and projected onto the A–M plane of Figure 6a shows only insignificant differences between the two plots; hence we will use orthogonal projections onto the M–T and M–A planes to show compositional variation. Figure 6b shows the M–T plot with all compositions of Table 4 and Sokolova & Hawthorne (2008); for simplicity, we omit compositions [0] and [7] from subsequent plots.

TABLE 4. CHEMICAL COMPOSITIONS OF INTEREST IN FIGURES 5 AND 6

[0]	Na_4		$[Al_2 Si_{10} O_{24}]$	(CO_3)
[1]	Na_4		$[Al_3 Si_9 O_{24}]$	Cl
(2)	Na_3	Ca	$[Al_5 Si_5 O_{24}]$	(CO_3)
(3)	Na_3	Ca	$[Al_4 Si_6 O_{24}]$	Cl
(4)	Na	Ca_3	$[Al_8 Si_7 O_{24}]$	(CO_3)
(5)	Na	Ca_3	$[Al_6 Si_6 O_{24}]$	Cl
[6]		Ca_4	$[Al_6 Si_6 O_{24}]$	(CO_3)
[7]		Ca_4	$[Al_7 Si_5 O_{24}]$	Cl

Figure 7 shows the variations in Al and (CO_3) + (SO_4) as functions of Ca content for the crystal structures refined by Sokolova & Hawthorne (2008). At the meionite end of the series, Al varies linearly with Ca content between compositions (4) and [6] (Fig. 7a), as indicated by Evans *et al.* (1969) and Zolotarev (1996). However, at lower Ca (and *Me*) content, the data are intermediate between the suggested trends of Evans *et al.* (1969) and Zolotarev (1996) (Fig. 7a). In this region, we may interpret the trend of the data in two ways: (1) as a smooth curve with maximum curvature at the phase transition, or (2) as two separate linear trends for the $I4/m$ marialite and the $P4_2/n$ scapolite, the two trends being noncollinear (*i.e.*, there is a discontinuity at the transition in symmetry).

It is important to emphasize that Figure 7a does not show the complete variation in chemical composition of scapolite-group minerals; there is also variation in the Cl and (CO_3) [and (SO_4)] contents. The variations in these constituents in the crystals examined here are shown in Figure 7b; the data show analogous deviations from the trends suggested by Evans *et al.* (1969) and Zolotarev (1996) as the data of Figure 7a. There is somewhat more scatter in the data of Figure 7b than in the data of Figure 7a, but this is not surprising, as the (CO_3) contents were calculated, whereas the rest of the data were measured. The variation in (CO_3) + (SO_4) content tends to favor a discontinuity at the transition. We may derive the substitutions on the linear segments of the trends in Figure 7, both with and without a discontinuity at ~Me_{22}; these are listed in Table 5.

In the above discussion, we described the character of the nonlinear compositional variation across the marialite–meionite series. However, we did not address the origins of this nonlinear variation. These will be examined later in this paper.

Short-Range Order at the *A* and *M* Sites

A key feature in the marialite–meionite series is the replacement of Cl by (CO_3) at the *A* site, and the corresponding replacement of Na by Ca at the *M* site. According to the extension of bond-valence theory to local (short-range) arrangements (Hawthorne 1997a), the sum of the local bond-valences incident at an *A*-site anion should obey the valence-matching principle (Brown 1981, Hawthorne 1994, 1997a, b). An important issue in this regard is the variation in *M–A* distance across the series; this variation is shown in Figure 8. With increasing Ca content, *M–A* increases rapidly in *I*-centered marialite, but the rate of change of *M–A* decreases at ~$Ca_{0.90}$ and then *M–A* varies linearly to Ca_4. From Figure 8, we may derive the following *M–A* distances for Me_0 (= Ca_0) and Me_{100} (= Ca_4): 2.89 and 3.22 Å, respectively. We will now consider the bond-valence implications of different possible local (short-range) arrangements as a function of bulk composition.

Short-range order: Cl at the A site

The *A* site is coordinated by four *M* cations. As we know the *M–A* distances, we may calculate the bond-valence incident at the *M* site for *M* = Cl with different cations occupying the adjacent *M*-sites, *i.e.*, for the *local* clusters Na_4Cl, Ca_4Cl and K_4Cl (assuming no relaxation). The variations in these sums are shown as a function of bulk composition in Figure 9; the

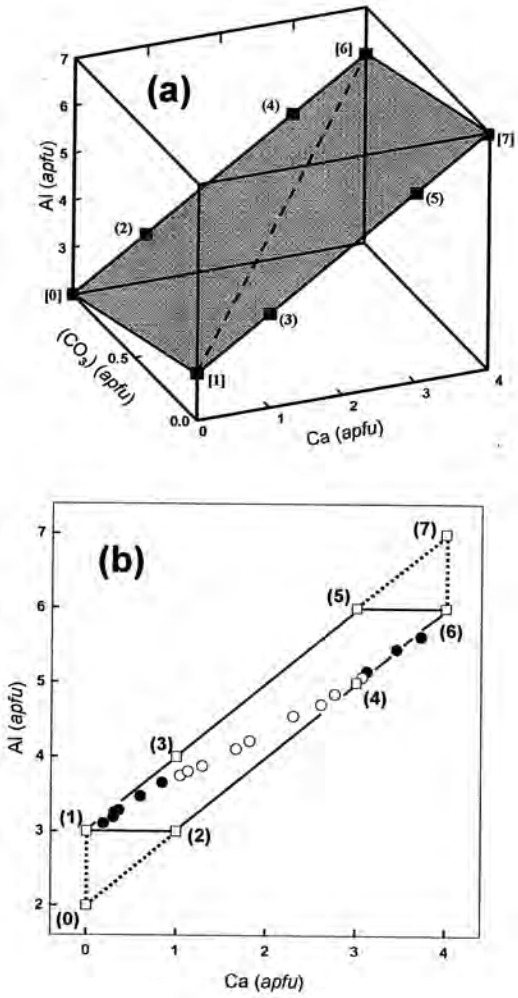

FIG. 6. (a) Al–Ca–(CO_3) composition space in *apfu*; the scapolite structure is constrained to the grey plane; (b) variation in total Al *(apfu)* as a function of Ca content (*apfu*) across the marialite–meionite series; all end-member compositions listed in Table 3 are shown as squares.

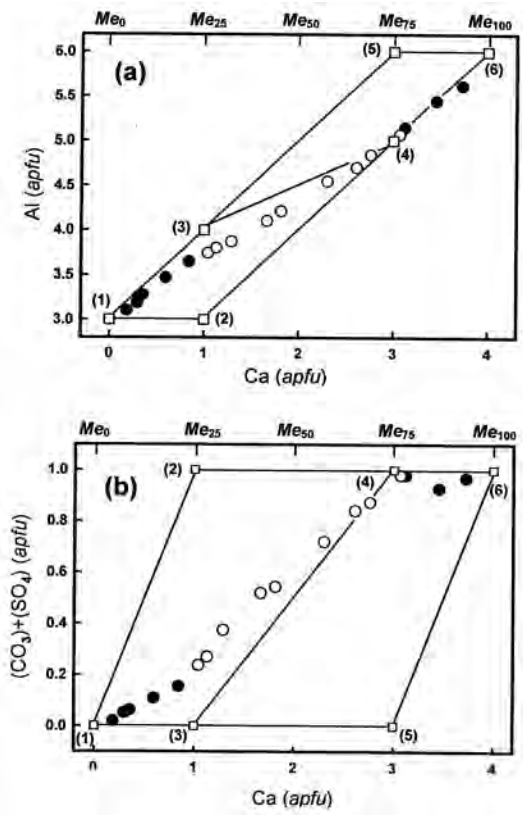

FIG. 7. Compositional variation across the marialite–meionite series: (a) Variation in total Al *(apfu)* as a function of Ca content (*apfu*); (b) Variation in (CO_3) + (SO_4) *(apfu)* as a function of Ca content (*apfu*); black circles: *I*4/*m* structures; white circles: $P4_2/n$ structures; numbered squares: compositions of Table 3.

broken horizontal line shows the ideal bond-valence incident at the *A* site where occupied by a Cl anion, *i.e.*, 1.0 *vu*. The incident bond-valence at Cl in the local arrangement Na_4Cl varies from ~0.25 to 0.55 *vu*; it never approaches the ideal value of 1 *vu*, even at the end-member marialite composition. The incident bond-valence at Cl in the local arrangement Ca_4Cl varies from ~0.45 to 1.00 *vu*, approaching the ideal value of 1 *vu* at the end-member marialite composition (which ironically contains no Ca). The incident bond-valence at Cl in the local arrangement K_4Cl varies from ~0.70 to 1.50 *vu*, attaining the ideal value of 1 *vu* at a composition of ~$Ca_{0.90}$. Figure 9 shows that the bond-valence requirements of Cl at the *A* site can never be satisfied in the marialite–meionite series (except for local arrangements involving K). So what happens?

Consider first the situation in Me_0 with an *M–A* distance of 2.89 Å. The resulting sum of the incident bond-valences at *A* (= Cl) is 0.135 × 4 = 0.54 *vu*; this value is significantly less that the value of 1.0 *vu* required by the valence-matching principle (Brown 1981, Hawthorne 1994, 1997b), and above we suggested that Cl is dynamically disordered within the *A* cavity as a response to this problem. The existence of marialite close to end-member composition [*i.e.*, composition S(1)] indicates that the structure can accommodate an incident bond-valence sum of ~0.50 *vu* at Cl.

Consider next the incorporation of Cl at the *A* site in a composition close to Me_{100}. The *M–A* distance at Me_{100} is 3.22 Å; this corresponds to a Ca–Cl bond-valence of 0.101 *vu*, which would give an incident bond-valence of 0.404 *vu* at Cl. This value suggests that the cavity surrounding the *A* site is too large at these compositions to incorporate Cl, such that the bond-valence requirements of this anion can be satisfied (even with disorder off the central *A* site). For K at the *M* site, the K–Cl bond-valence for Me_{100} is 0.151 *vu*, and for Me_{75}, it is 0.180 *vu*; this gives incident bond-valence sums at the *A* site of 0.604 and 0.72 *vu*. These values are in the range of the analogous values in marialite and suggest that small amounts of Cl may be incorporated into *I*-centered meionite *via* coordination by K at the *A* site. Examination of the chemical compositions of crystals S(15)–S(18) (Fig. 10) shows that the amount of Cl in these crystals is positively correlated with the amount of K present. Moreover, the slope of the line in Figure 10 suggests that Cl is incorporated into the structure as clusters of the form $\{ClK_2Ca_2\}$ in *I*-centered meionite.

TABLE 5. EXCHANGE REACTIONS FOR CHEMICAL VARIATION IN THE SCAPOLITE-GROUP MINERALS

with discontinuity at Na_3Ca			
Ca: 0–1	$Ca + Al_{0.78} + (CO_3)_{0.22}$	↔	$Na + Si_{0.78} + Cl_{0.22}$
Ca: 1–3	$Ca + Al_{0.64} + (CO_3)_{0.36}$	↔	$Na + Si_{0.64} + Cl_{0.36}$
Ca: 3–4	$Ca + Al$	↔	$Na + Si$
without discontinuity at Na_3Ca			
Ca: 0–1	$Ca + Al_{0.75} + (CO_3)_{0.25}$	↔	$Na + Si_{0.75} + Cl_{0.25}$
Ca: 1–3	$Ca + Al_{0.625} + (CO_3)_{0.375}$	↔	$Na + Si_{0.625} + Cl_{0.375}$

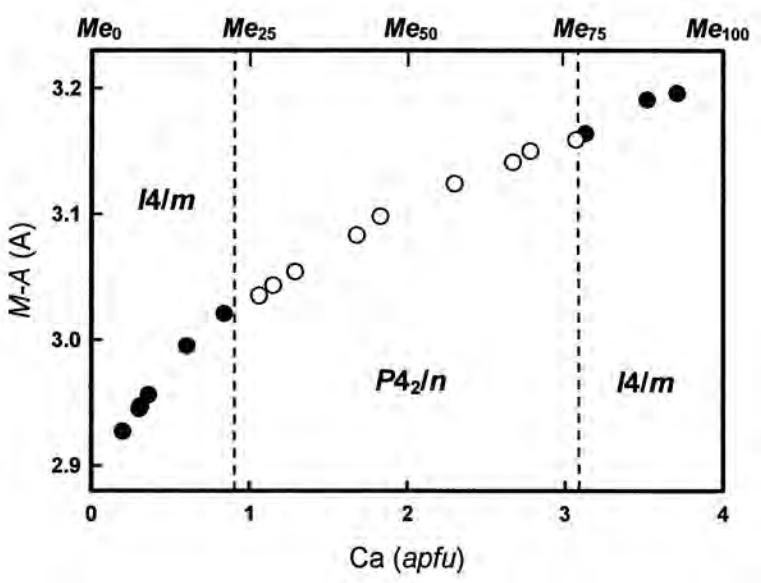

FIG. 8. Variation in *M–A* distance as a function of Ca content in the marialite–meionite series; legend as in Figure 3.

Short-range order: (CO_3) at the A site

For *I*-centered marialite, we do not know the distances involving the *M* site and the O anions of the (CO_3) because the low (CO_3) content at these compositions precludes location of the relevant partly occupied sites; the closest composition at which there is any information is crystal S(8). Using the observed *M*–O bond-lengths, we may calculate the net bond-valences incident at the (CO_3) group as a function of bulk composition for the local clusters (CO_3)Na_4 and (CO_3)Ca_4 (Fig. 11). For compositions close to Me_{25}, the cluster (CO_3)Na_4 shows reasonable agreement with the valence-sum rule (~2.0 *vu*), falling to ~1.1 *vu* at Me_{100}. For compositions close to Me_0, the cluster (CO_3)Ca_4 deviates strongly from the valence-sum rule (~3.0 *vu*), falling to ~2 *vu* at Me_{88}. The effect of mixed clusters, (CO_3)(Na,Ca)$_4$ may be evaluated by interpolation in Figure 11. The dotted line in Figure 11 shows the long-range bond-valence incident at the (CO_3) group; note that it agrees with the valence-sum rule close to ~Me_{50}.

The Effect of SRO on Chemical Variation Across the Series

Inspection of Figure 11 shows that in *I*-centered meionite, the bond-valence requirements of the (CO_3) group are satisfied through coordination by Ca_4 close to Me_{100} and by Ca_3Na as the *Me* content decreases. Also, any attempt to introduce Cl at the *A* site (except in the presence of K), leads to very low local incident bond-valence sums at Cl. Both of these observations indicate that Na can replace Ca but Cl cannot replace (CO_3) in *I*-centered meionite, and hence the Na–Ca substitution must be charge-compensated by substitution of Al by Si: Na + Si → Ca + Al, as is observed (Fig. 7a, Table 4). At some stage, contraction of the structure allows incorporation of Cl; because of the probable dynamic disorder of Cl in the structure, it is impossible to state convincingly at what composition this change should occur, but observation indicates this to be at ~Me_{75}, close to the composition at which the change in symmetry from *I*4/*m* to *P*4$_2$/*n* occurs. Inspection of Figure 11 indicates that as the Ca content of scapolite decreases, the coordination required to satisfy the local bond-valence requirements of the (CO_3) group changes from Ca_3Na at ~Me_{75} to Ca_2Na_2 at ~Me_{50} to $CaNa_3$ to Na_4 at ~Me_{20}. This variation suggests a change in composition from ~Me_{75} to Me_0 that is linear from composition (4) to composition [1] (Fig. 7). The observed change is similar to this, but shows a kink at ~Me_{20} where the symmetry change occurs, suggesting that the change in symmetry perturbs the mechanism suggested above.

Coupling Between the [(Al,Si)$_{12}O_{30}$] and {Na,Ca}{Cl,(CO_3)} Frameworks: Short-Range Order

Although we have not yet examined the details of the mechanism driving the *I*4/*m* ⇄ *P*4$_2$/*n* phase transition in scapolite, we may make some observations that pertain

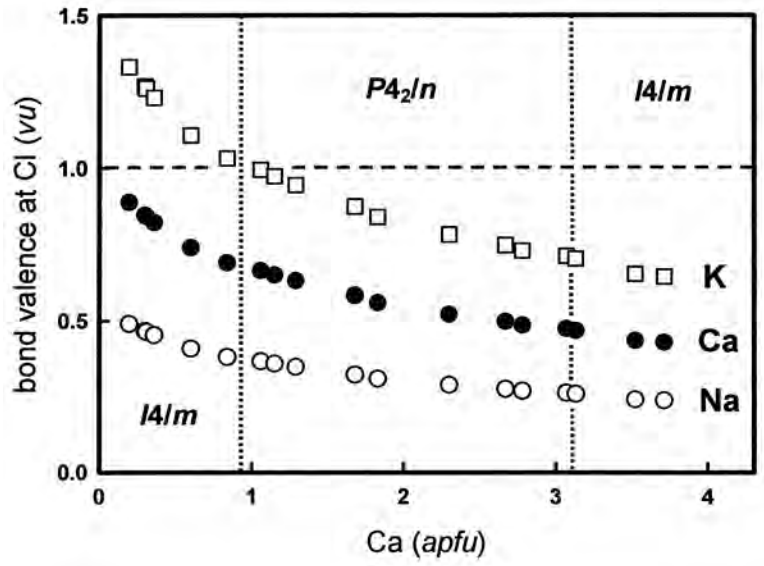

FIG. 9. Variation in bond valence locally incident at Cl (at the *A* site) for different short-range clusters, Na_4Cl, K_4Cl and Ca_4Cl; the broken horizontal line shows agreement with the *local* valence-sum rule.

to this mechanism. The first important feature of this transition is that it is symmetrical with respect to variation in chemical composition. This behavior is quite different from that in most phase transitions in framework aluminosilicate minerals (*e.g.*, K-feldspar – albite, albite – anorthite) in that the space group is the same at each end of the series and different at intermediate compositions, and suggests that the underlying cause of the transitions must also have a similar symmetry.

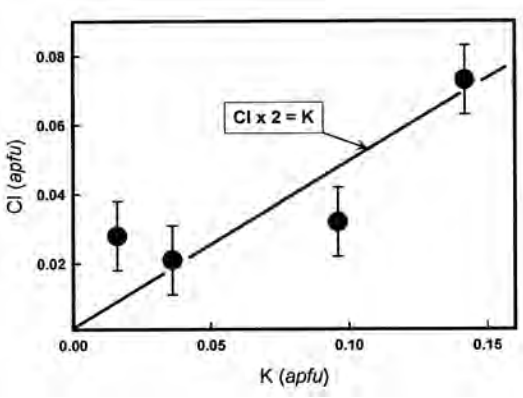

FIG. 10. Variation in Cl content as a function of K content in meionite crystals S(15)–S(18); the horizontal line is drawn through zero with a slope of 2 (*i.e.*, Cl = 2.0 K).

So far, we have identified two different issues affecting the scapolite structure: (1) the misfit between the two interpenetrating frameworks, and (2) extensive SRO associated with the $\{Na,Ca\}_4\{Cl,(CO_3)\}$ framework. The variation in patterns of SRO around the *A* site, Na_4 to $CaNa_3$ to Ca_2Na_2 to Ca_3Na to Ca_4, shows a similar symmetry as a function of bulk composition, suggesting that this SRO is involved in the origin of the phase transitions in scapolite. The $[(Al,Si)_{12}O_{30}]$ and $\{Na,Ca\}_4\{Cl,(CO_3)\}$ frameworks link by sharing O atoms with *M* cations of one framework and *T* cations of the other framework. Thus SRO that affects the *A* anions and *M* cations of the $\{Na,Ca\}_4\{Cl,(CO_3)\}$ framework should propagate through the linking O atoms to affect the *T* cations of the $[(Al,Si)_{12}O_{30}]$ framework.

Local bond-valences around the T(2) site

The topological symmetry of the scapolite structure is *I*4/*m*. Let us examine the bond-valence incident at the *T*(2) site in this structural arrangement; this is illustrated in Figure 12.

The bond valence incident at the *T*(2) tetrahedron is (approximately) as follows:

$$\{2M + M' + 2M''\} + \{T(1) + \{T(2)' + T(2)'' + T(2)'''\}\ vu \qquad (3)$$

where *M*, *M*′, *M*″, *T*(1), *T*(2)′, *T*(2)″ and *T*(2)‴ represent the bond valences at the corresponding sites. We will take these bond valences from the

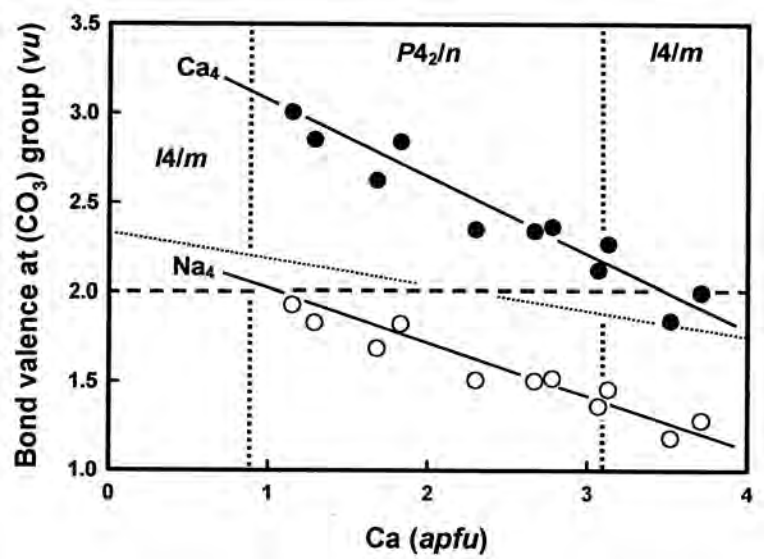

FIG. 11. Variation in bond valences locally incident at (CO_3) for the short-range clusters $(CO_3)Na_4$ and $(CO_3)Ca_4$; the broken horizontal line shows agreement with the local valence-sum rule.

bond-valence tables of the unstrained end-member structures (Table 1). The aggregate charge at the $T(2)$ tetrahedron is $8^- - Z^{T(2)}$ (the formal charge of the four simple anions) minus the formal charge at the $T(2)$ site. The local version of the valence-sum rule (Hawthorne 1997a) requires that

$$\Sigma M + \Sigma T = 8^- - Z^{T(2)} \quad (4)$$

where $\Sigma M = 2M + M' + 2M''$ and $\Sigma T = T(1) + T(2)' + T(2)'' + T(2)'''$. We may write equation (4) for $T(2)$ = Al and Si, respectively:

$$T(2) = \text{Al: } \Sigma M + \Sigma T = 5\ vu \quad (5a)$$

$$T(2) = \text{Si: } \Sigma M + \Sigma T = 4 \quad (5b)$$

Possible values for ΣM and ΣT are listed below:

ΣM	2Na + Na + 2Na	0.642 *vu*
	2Na + Ca + 2Na	0.664
	2Ca + Na + 2Na	0.844
	2Ca + Ca + 2Na	0.866
	2Ca + Na + 2Ca	1.046
	2Ca + Ca + 2Ca	1.068
ΣT	Si + Si + Si + Si	4.000 *vu*
	Si + Si + Si + Al	3.750
	Si + Si + Al + Al	3.500
	Si + Al + Al + Al	3.250
	Al + Al + Al + Al	3.000

The values corresponding more closely to equation (5a) are as follows:

2Ca + Ca + 2Ca + Si + Si + Si + Si = 1.068 + 4.000 = 5.068 *vu*

2Ca + Na + 2Ca + Si + Si + Si + Si = 1.046 + 4.000 = 5.046

2Ca + Ca + 2Na + Si + Si + Si + Si = 1.866 + 4.000 = 4.866

2Ca + Na + 2Na + Si + Si + Si + Si = 1.844 + 4.000 = 4.844

2Na + Ca + 2Na + Si + Si + Si + Si = 1.664 + 4.000 = 4.664

2Na + Na + 2Na + Si + Si + Si + Si = 1.642 + 4.000 = 4.642

The arrangements most in accord with the valence-matching principle are the arrangements most likely

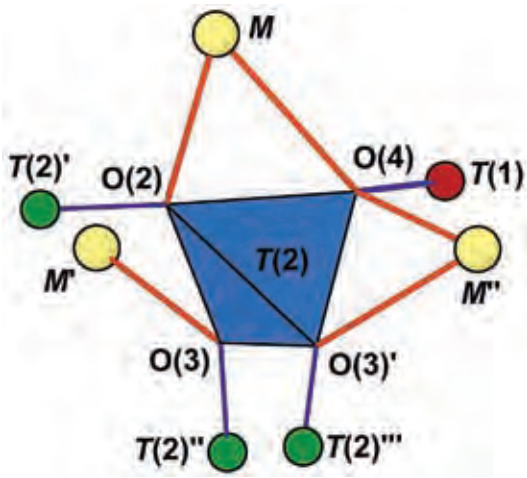

FIG. 12. The coordination of the $T(2)$ tetrahedron in the *I*4/*m* scapolite structure; the structure fragment is oriented to show most clearly the coordinating sites; legend as in Figure 1, except the $T(1)$ site is shown as a red circle.

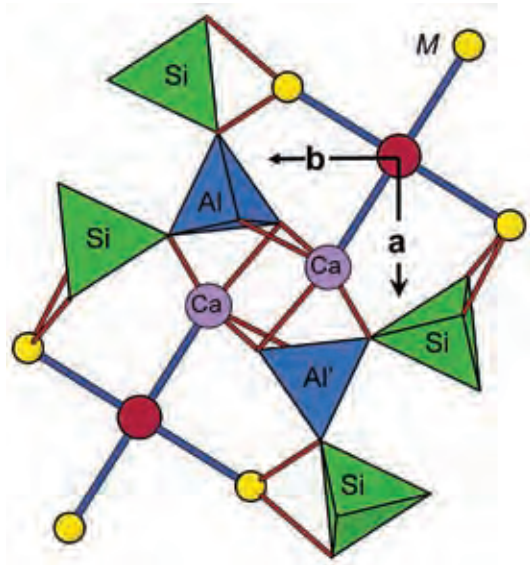

FIG. 13. The local association of Ca at M and Al at $T(2)$ in the *I*4/*m* scapolite structure; the red circle represents the *A* site, which may be occupied by Cl or (CO_3), $^{T(2)}$Al and $^{T(2)}$Si tetrahedra are blue and green, respectively, Ca atoms are shown as mauve circles, and M cations (not identified as Na or Ca) are shown as yellow circles.

to occur *if* these arrangements are in accord with the bulk composition of the crystal. For example, at Me_0, there is no Ca in the crystal; thus arrangement 2Na + Na + 2Na + Si + Si + Si + Si is the only arrangement possible, even though it does not agree very well with the valence-matching principle (perhaps accounting for the rarity of scapolite crystals of this composition). In the presence of abundant Ca, $T(2)$ = Al will be associated with Ca at the M and M'' sites and either Ca or Na at the M' site, and Si at the $T(1)$, $T(2)'$, $T(2)''$ and $T(2)'''$ sites (Fig. 12). The situation for Si at the $T(2)$ site is somewhat less constrained. The values corresponding most closely to equation (5b) are as follows:

2Na + Na + 2Na + Si + Al + Al + Al = 0.642 + 3.250 = 3.892 *vu*

2Na + Ca + 2Na + Si + Al + Al + Al = 0.664 + 3.250 = 3.914

2Ca + Na + 2Na + Si + Al + Al + Al = 0.844 + 3.250 = 4.094

2Ca + Ca + 2Na + Si + Al + Al + Al = 0.866 + 3.250 = 4.116

2Ca + Na + 2Ca + Al + Al + Al + Al = 1.046 + 3.000 = 4.046

2Ca + Ca + 2Ca + Al + Al + Al + Al = 1.068 + 3.000 = 4.068

All these values correspond fairly closely to equation (5b). Perhaps the arrangement above with the largest deviation will not occur, but this is not critical to the argument. What is apparent is that the local arrangements are much less constrained where $T(2)$ is occupied by Si than where $T(2)$ is occupied by Al.

The constraint of bulk composition

The argument developed above indicates that for optimum agreement with the valence-sum rule, Al at $T(2)$ is locally associated with 5Ca and 4Si atoms. Any local association of cations such as this must also be compatible with the bulk composition of the crystal. Thus the end-member composition $Na_4[(^{T(1)}Si_4{}^{T(2)}(Si_5Al_3)O_{30}]Cl$ has no Ca to locally coordinate to Al at $T(2)$, and a very strained structure results. The situation is somewhat relieved at more Ca-rich compositions, but never does the bulk composition approach the $^{T(2)}$Al:Ca ratios of 1:4 and 1:5 that occur in the optimum arrangements described above. Of course, linking of these arrangements together alleviates this problem, but it does not solve it: across much of the series, there is a deficiency of Ca relative to Al, and the local arrangements described above link so as to take maximum advantage of the Ca, *i.e.*, locally associate Ca with $^{T(2)}$Al. Of great importance in this regard is the local association shown in Figure 13. Two Ca atoms occupy the M and M'' sites adjacent to the $T(2)$ tetrahedron occupied by Al (labeled Al in Fig. 13). Figure 13 also shows that the two Ca atoms at M and M'' also link to another $T(2)$ tetrahedron labeled Al', thereby maximizing the association of $^{T(2)}$Al with Ca and partly offsetting the fact that there is significantly more $^{T(2)}$Al than Ca in scapolite. This local association of two Ca atoms with two $^{T(2)}$Al tetrahedra is shown in Figure 13. The chemical species of the other M cations are not indicated, although it should be noted that both Na and Ca are compatible with the arrangements that are in accord with the valence-sum rule as discussed above.

The character of the AM_4 cluster

Above, we showed that the arrangements ANa$_4$, ANa$_3$Ca, ANa$_2$Ca$_2$, ANaCa$_3$ and ACa$_4$ are successively stable across the series from marialite to meionite. Inspection of Figures 1 and 13 indicates that propagation of the local association of Ca and Al shown in Figure 13 is dependent on the type of AM_4 cluster present, which in turn is dependent on the chemical composition of the structure. Figure 14 shows the approximate distribution of AM_4 clusters as suggested by the bond-valence arguments given above.

For the cluster ANa$_4$, the arrangement shown in Figure 13 cannot occur; Al at $T(2)$ must be associated with Na at M. For the cluster ANa$_3$Ca, the arrangement shown in Figure 13 can occur. However, all M sites shown in yellow in Figure 13 must be Na, and hence there are no constraints on the linkage of the clusters of Figure 13 to form an extended structure. Inspection of the linkages involving Si at $T(2)$ listed above indicates that all combinations of Na and Ca can participate in these linkages and give reasonable accord with the valence-matching principle. For the clusters ANaCa$_3$ and ACa$_4$, the arrangement shown in Figure 13 has Ca dominating the M sites; the situation is the inverse of that for ANa$_4$ and ANa$_3$Ca, respectively, in that disorder with regard to translational symmetry is propagated with further linkage.

For the cluster ANa$_2$Ca$_2$, the situation is somewhat more complicated, as this cluster may potentially occur in two configurations: (1) Na cations are *cis* and Ca cations are *cis*, and (2) Na cations are *trans* and Ca cations are *trans*. Let us consider first the *cis* configuration (Fig. 15), where the optimum arrangement involving Al at $T(2)$ (Fig. 13) is indicated by the broken-line box. The *cis* arrangement of the Ca atoms about the A site (which may be occupied by Cl or CO_3) can give rise to a variety of local arrangements, but none of them include the occurrence of another optimum arrangement around $^{T(2)}$Al within the same unit cell, *i.e.,* a long-range ordered arrangement with the same unit-cell is not possible.

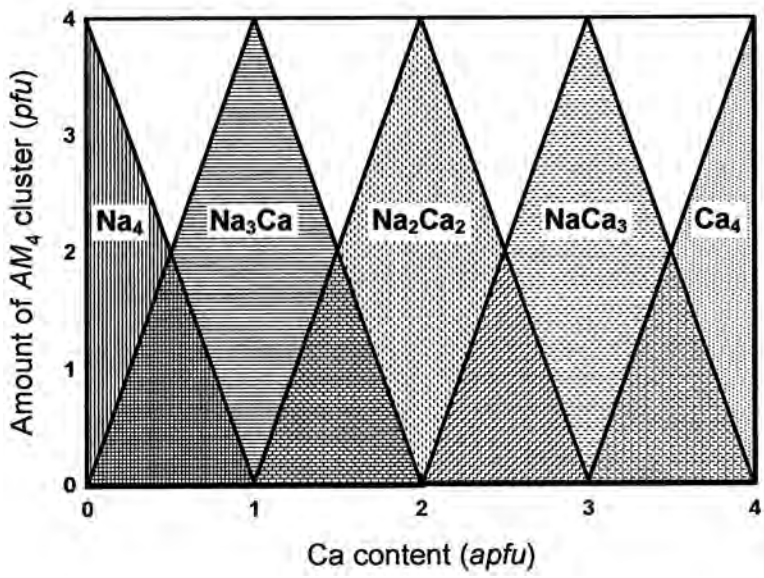

FIG. 14. The distribution of AM_4 clusters across the marialite–meionite join.

Consider next the *trans* configuration (Fig. 16). The *trans* arrangement of the Ca atoms about the *A* site allows repetition of the optimum local arrangement around $^{T(2)}$Al *trans* to the original arrangement. Moreover, Na is locally associated with Si at *T*(2), allowing the maximum possible association of $^{T(2)}$Al with Ca for a specific bulk-composition.

Local arrangements and long-range symmetry

Inspection of Figure 16 shows that the translational symmetry of the original (*I*4/*m*) cell is maintained in terms of the order of Al and Si. This means that the arrangement shown in Figure 16 is repeated in the *ab* plane by the *a* and *b* translations of the cell. However, the original *I*4/*m* symmetry cannot be maintained as there is now long-range order of Al and Si at what was the *T*(2) site in the *I*4/*m* structure, and a new space-group symmetry must result. Consider the two *T*(2) sites in the upper part of the dashed rectangle in Figure 16: we will label these $^{Al}T(2)$ and $^{Si}T(2)$ and recognize that these must be distinct sites in the new structure. The coordinates of these two sites in the original (*I*4/*m*) cell are as follows: $^{Al}T(2)$: 0.084 0.659 0.299; $^{Si}T(2)$: 0.164 0.412 0.211. To help in the following argument, the symmetry operations and their labels are shown in Table 6. Comparison of the coordinates of $^{Al}T(2)$ and $^{Si}T(2)$ with the coordinates of the *I*4/*m* structure (Sokolova & Hawthorne 2008, Table 6) shows that the coordinates of $^{Al}T(2)$ and $^{Si}T(2)$ are related to the *T*(2) site by the symmetry operations $*\bar{4}^3$ and E, respectively. The key issue here is that the symmetry element relating $^{Al}T(2)$ to $^{Si}T(2)$ in the original *I*4/*m* space group is lost because of the order of Al and Si, and hence the space group of the ordered arrangement must change.

We may derive the space group of the new arrangement by removing the symmetry element $*\bar{4}^3$ from the space group *I*4/*m*. Table 7 shows the multiplication table for space group *I*4/*m*; the row and column for $*\bar{4}^3$ are deleted (as shown by the dark ribbons). One of the axioms of group theory is that the product of any two elements of the group must be an element of the group. Thus as we have deleted the column and row for $*\bar{4}^3$, we must also delete all rows and columns that contain this element; these deletions are shown by the pale ribbons in Table 7. The result is the multiplication table for the space group $P4_2/n$. One must be a little more specific here, as the space group *I*4/*m* has two distinct $P4_2/n$ subgroups (Stokes & Hatch 1988). However, one of these is a klassengleich IIa group and the other is a klassengleich IIb group (Burns & Glazer 1990). Above, we show that the unit cell is maintained in this transition, and hence the derivative cell is a klassengleich IIa group. Moreover, inspection of Stokes & Hatch (1988) shows that the klassengleich $P4_2/n$ subgroup involves a change in origin of 1/4 1/4 1/4 relative to the origin in *I*4/*m* (*cf.* Sokolova & Hawthorne 2008, Tables 5, 6). Thus the transitions are driven by the coupling between short-range order in the $\{Na,Ca\}_4\{Cl,(CO_3)\}$ and $[(Al,Si)_{12}O_{30}]$ frameworks. The order of Al and Si over what becomes the *T*(2) and *T*(3) sites in the $P4_2/n$ structure drives the transition, whereas because the *M*

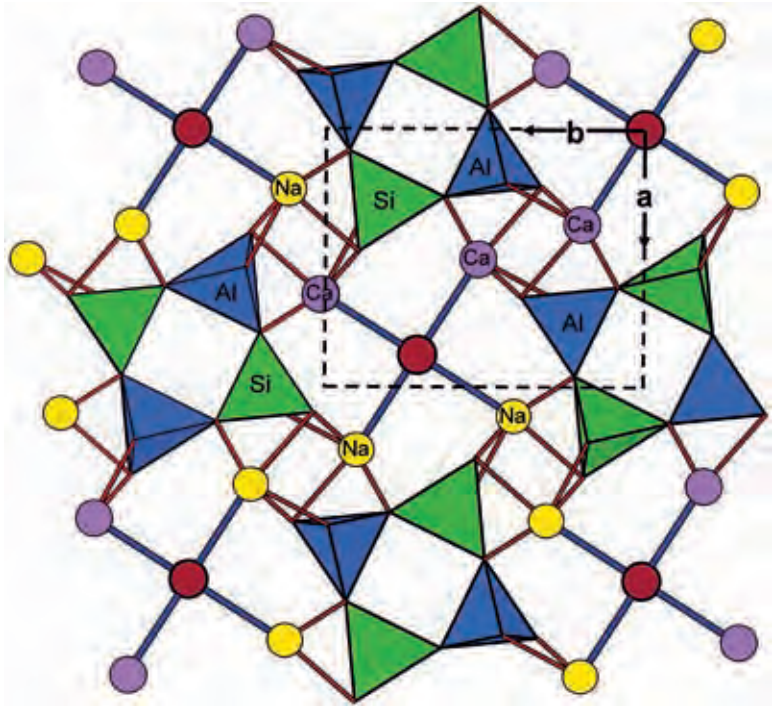

FIG. 15. The local association of Ca at *M* and Al at *T*(2) (outlined by the broken-line box) in combination with the *cis* ANa_2Ca_2 cluster. Note that translational symmetry is not maintained; legend as in Figure 13, where Na is at the *M* site (yellow circles; this is indicated by the letters Na.).

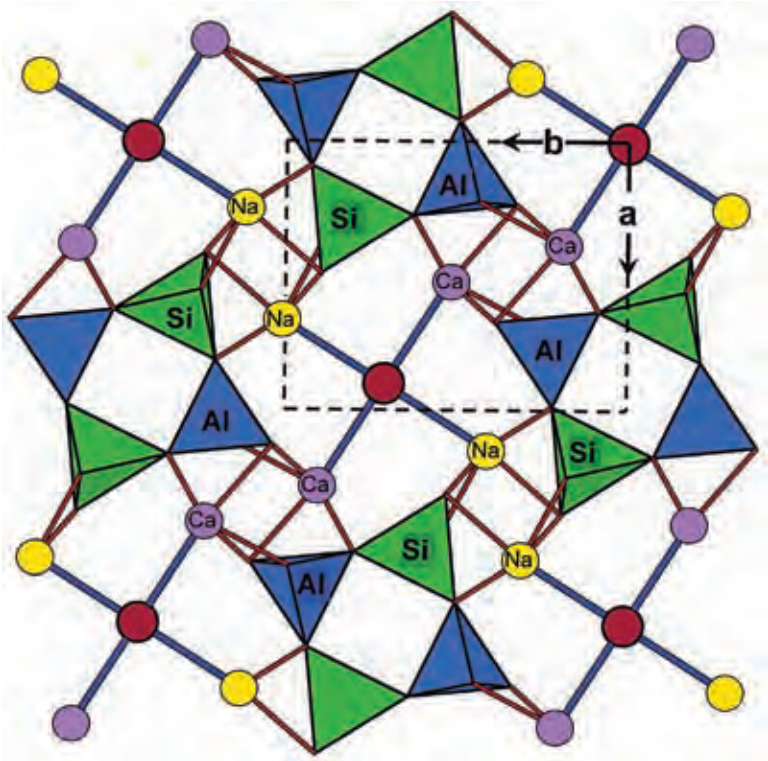

FIG. 16. The local association of Ca at *M* and Al at *T*(2) (outlined by the broken-line box) in combination with the *trans* ANa_2Ca_2 cluster. Note that translational symmetry is maintained; legend as in Figure 15.

site remains of the same equipoint rank in $P4_2/n$ as in $I4/m$, the (short-range) order of Na and Ca does not become apparent in the (long-range) $P4_2/n$ structure.

Chemical compositions at the phase transitions

The reason for the symmetrical nature of the $I4/m \rightleftarrows P4_2/n$ phase transitions now becomes apparent. The driving mechanism for the lowering of symmetry is the coupled ordering between the $\{Na,Ca\}_4\{Cl,(CO_3)\}$ and $[(Al,Si)_{12}O_{30}]$ frameworks. However, as the composition of the $\{Na,Ca\}_4\{Cl,(CO_3)\}$ framework deviates in either direction from the composition Na_2Ca_2, the effectiveness of this mechanism decreases and becomes zero at compositions Na_3Ca and $NaCa_3$, where local Na_2Ca_2 arrangements either vanish or occur in sufficiently low numbers that they do not propagate their orientation sufficiently to form a coherently diffracting volume that reflects a lowering of symmetry.

TABLE 6. SYMMETRY OPERATIONS OF THE SPACE GROUP *I4/m*

x	y	z	E	½ + x	½ + y	½ + z	I
y	$\bar{x}$	z	4^1	½ − x	½ − y	½ + z	2_1
$\bar{x}$	$\bar{y}$	z	4^2	½ + x	½ + y	½ − z	n
$\bar{y}$	x	z	4^3	½ − x	½ − y	½ − z	*i
x	y	$\bar{z}$	m	½ + y	½ − x	½ + z	$4'_{2_1}$
$\bar{x}$	$\bar{y}$	$\bar{z}$	i	½ − y	½ + x	½ + z	$4^3_{2_1}$
$\bar{y}$	x	$\bar{z}$	$\bar{4}^1$	½ + y	½ − x	½ − z	$*\bar{4}^1$
y	$\bar{x}$	$\bar{z}$	$\bar{4}^3$	½ − y	½ + x	½ − z	$*\bar{4}^3$

SUMMARY

We have addressed many different issues in the crystal chemistry of the marialite–mieionite series. For clarity, these are summarized below:

(1) There are three distinct compositional series between end-member marialite (Me_0) and end-member meionite (Me_{100}) (*cf.* Zolotarev 1996, Teertstra & Sherriff 1996, Seto *et al.* 2004):

[1] Ca: 0–1 [Me_0–$Me_{0.25}$] $Ca + Al_{0.78} + (CO_3)_{0.22} \rightleftarrows Na + Si_{0.78} + Cl_{0.22}$

[2] Ca: 1–3 [Me_{25}–Me_{75}] $Ca + Al_{0.64} + (CO_3)_{0.36} \rightleftarrows Na + Si_{0.64} + Cl_{0.36}$

[3] Ca: 3–4 [Me_{75}–Me_{100}] $Ca + Al \rightleftarrows Na + Si$

There is a slight discontinuity at the transition composition $Me_{0.25}$, a result of accumulated strain in the $I4/m$ marialite structure close to the transition composition.

(2) The scapolite structure consists of two interpenetrating frameworks, an $[(Al,Si)_{12}O_{24}]$ framework and a $[\{Na,Ca\}_4\{Cl,(CO_3)\}]$ framework. The intrinsic (unstrained) dimensions of each framework are signifi-

TABLE 7. MULTIPLICATION TABLE FOR THE SPACE GROUP *I4/m*

	E	4^1	4^2	4^3	i	m	$\bar{4}^1$	$\bar{4}^3$	I	2_1	n	*i	$4'_{2_1}$	$4^3_{2_1}$	$*\bar{4}^1$	$*\bar{4}^3$
E	E	4^1	4^2	4^3	i	m	$\bar{4}^1$	$\bar{4}^3$	I	2_1	n	*i	$4'_{2_1}$	$4^3_{2_1}$	$*\bar{4}^1$	$*\bar{4}^3$
4^1	4^1	4^2	4^3	E	4^1	4^3	m	i	$4'_{2_1}$	$4^3_{2_1}$	$*\bar{4}^1$	$*\bar{4}^3$	2_1	I	*i	n
4^2	4^2	4^3	E	4^1	m	i	$\bar{4}^3$	$\bar{4}^1$	2_1	I	*i	n	$4'_{2_1}$	$4^3_{2_1}$	$*\bar{4}^1$	$*\bar{4}^3$
4^3	4^3	E	4^1	4^2	$\bar{4}^3$	$\bar{4}^1$	I	m	$4^3_{2_1}$	$4'_{2_1}$	$*\bar{4}^3$	$*\bar{4}^1$	I	2_1	n	*i
i	i	4^1	m	$\bar{4}^3$	E	4^2	4^1	4^3	*i	n	2_1	I	$*\bar{4}^3$	$*\bar{4}^1$	$4^3_{2_1}$	$4'_{2_1}$
m	m	$\bar{4}^3$	i	$\bar{4}^1$	4^2	E	4^3	4^1	n	*i	I	2_1	$*\bar{4}^1$	$*\bar{4}^3$	$4'_{2_1}$	$4^3_{2_1}$
$\bar{4}^1$	$\bar{4}^1$	m	$\bar{4}^3$	i	4^1	4^3	4^2	E	$*\bar{4}^3$	$*\bar{4}^1$	$4^3_{2_1}$	$4'_{2_1}$	n	*i	I	2_1
$\bar{4}^3$	$\bar{4}^3$	i	$\bar{4}^1$	m	4^3	4^1	E	4^2	$*\bar{4}^1$	$*\bar{4}^3$	$4'_{2_1}$	$4^3_{2_1}$	*i	n	2_1	I
I	I	$4'_{2_1}$	2_1	$4^3_{2_1}$	*i	n	$*\bar{4}^3$	$*\bar{4}^1$	E	4^2	m	i	4^1	4^3	4^3	4^1
2_1	2_1	$4^3_{2_1}$	I	$4'_{2_1}$	n	*i	$*\bar{4}^1$	$*\bar{4}^3$	4^2	E	i	m	4^3	4^1	4^1	4^3
n	n	$*\bar{4}^3$	*i	$*\bar{4}^1$	2_1	I	$4^3_{2_1}$	$4'_{2_1}$	m	i	E	4^2	$\bar{4}^3$	$\bar{4}^1$	4^1	4^3
*i	*i	$*\bar{4}^3$	n	$*\bar{4}^1$	I	2_1	$4'_{2_1}$	$4^3_{2_1}$	I	m	4^2	E	$\bar{4}^1$	$\bar{4}^3$	4^3	4^1
$4'_{2_1}$	$4'_{2_1}$	2_1	$4^3_{2_1}$	I	$*\bar{4}^3$	$*\bar{4}^1$	n	*i	4^1	4^3	$\bar{4}^3$	$\bar{4}^1$	4^2	E	i	m
$4^3_{2_1}$	$4^3_{2_1}$	I	$4'_{2_1}$	2_1	$*\bar{4}^1$	$*\bar{4}^3$	i	n	4^3	4^1	$\bar{4}^1$	$\bar{4}^3$	E	4^2	m	i
$*\bar{4}^1$	$*\bar{4}^3$	*i	$*\bar{4}^3$	n	$4^3_{2_1}$	$4'_{2_1}$	I	2_1	$\bar{4}^3$	$\bar{4}^1$	4^1	4^3	i	m	4^2	E
$*\bar{4}^3$	$*\bar{4}^1$	n	$*\bar{4}^1$	*i	$4'_{2_1}$	$4^3_{2_1}$	2_1	I	4^3	4^1	4^1	4^3	m	i	E	4^2

The symmetry element $*\bar{4}^1$ [that is lost because of the order of Al and Si over adjacent *T*(2) sites (Fig. 11)] is deleted (dark shaded strip), together with the other elements as required by the properties of a group.

cantly different, as determined by the valence-matching principle and distance least-squares refinement, and there is an intrinsic steric stress between the two frameworks.

(3) The resulting structural strain results in deviations between the observed bond-valence sums incident at both cations and anions and the ideal sums calculated for a strain-free structure; these strains are a function of chemical composition across the series.

(4) Additional evidence of such structural strain is the large U_{eq} values for Cl at the *A* site across the series, and the large U_{eq} values for Na,Ca at the *M* site at the Na-rich part of the series (Fig. 3).

(5) Bond-valence considerations indicate extensive SRO (Short-Range Order) about both Cl and (CO_3) in scapolite. In particular, Cl cannot occur in *I*4/*m* meionite except where K is present; in this case, chemical variations indicate that Cl enters the *I*4/*m* meionite structure as $\{ClK_2Ca_2\}$ clusters.

(6) The bond-valence requirements of the (CO_3) group are satisfied by coordination Ca_4 at ~Me_{100}, Ca_3Na at ~Me_{75}, Ca_2Na_2 at ~Me_{55}, $CaNa_3$ at ~Me_{40}, and Na_4 at ~Me_{20}.

(7) The driving mechanism for the $I4/m \rightarrow P4_2/n$ transition is the coupling of SRO between the $[(Al,Si)_{12}O_{24}]$ framework and the $[\{Na,Ca\}_4\{Cl,(CO_3)\}]$ framework. This coupling is optimal for the composition Ca_2Na_2, where there is maximal Al–Si order between the *T*(2) and *T*(3) sites, decreases with increasing Ca or Na to either side of this central composition, and becomes zero at compositions Ca_3Na or $CaNa_3$ (*i.e.,* at ~Me_{75} and ~Me_{20}, where the $P4_2/n \rightarrow I4/m$ transitions occur), where the local Ca_2Na_2 clusters vanish.

Acknowledgements

This paper and its companion are dedicated to Joe Smith in recognition of his major contributions to the crystallography of rock-forming minerals.

We thank the reviewers for their comments and Editor Bob for his directions. This work was supported by a Canada Research Chair in Crystallography and Mineralogy and by Major Facilities Access, Major Equipment, Equipment and Discovery Grants to FCH from the Natural Sciences and Engineering Research Council of Canada.

References

Aitken, B.G., Evans, H.T., Jr. & Konnert, J.A. (1984): The crystal structure of a synthetic meionite. *Neues Jahrb. Mineral., Abh.* **149**, 309-342.

Baerlocher, C., Hepp, A. & Meier, W.M. (1977): DLS–76. *A Program for the Simulation of Crystal Structures by Geometric Refinement*. Institute of Crystallography and Petrography, Zurich, Switzerland.

Belokoneva, E.L., Sokolova, N.V. & Dorokhova, G.I. (1991): Crystal structure of natural Na,Ca-scapolite – an intermediate member of the marialite–meionite series. *Sov. Phys. Crystallogr.* **36**, 828-830.

Belokoneva, E.L., Sokolova, N.V. & Urusov, V.S. (1993): Scapolites – crystalline structures of marialite (Me_{11}) and meionite (Me_{88}), space group as a function of composition. *Crystallogr. Rep.* **38**, 25-28.

Brese, N.E. & O'Keeffe, M. (1991): Bond-valence parameters for solids. *Acta Crystallogr.* **B47**, 192-197.

Brown, I.D. (1981): The bond-valence method: an empirical approach to chemical structure and bonding. *In* Structure and Bonding in Crystals II (M. O'Keeffe & A. Navrotsky, eds.). Academic Press, New York, N.Y. (1-30).

Brown, I.D. (2002): *The Chemical Bond in Inorganic Chemistry. The Bond Valence Model*. Oxford Scientific Publications, Oxford, U.K.

Burns, G. & Glazer, A.M. (1990): *Space Groups for Solid State Scientists*. Academic Press, San Diego, California.

Buseck, P.R. & Iijima, S. (1974): High resolution electron microscopy of silicate. *Am. Mineral.* **59**, 1-24.

Chamberlain, C.P., Docka, J.A., Post, J.E. & Burnham, C.W. (1985): Scapolite: alkali atom configurations, antiphase domains, and compositional variations. *Am. Mineral.* **70**, 134-140.

Comodi, P., Mellini, M. & Zanazzi, P.F. (1990): Scapolites: variation of structure with pressure and possible role in the storage of fluids. *Eur. J. Mineral.* **2**, 195-202.

Evans, B.W., Shaw, D.M. & Haughton, D.R. (1969): Scapolite stoichiometry. *Contrib. Mineral. Petrol.* **24**, 293-305.

Gossner, B. & Brükkl, K. (1928): Untersuchungen über die Skapolithgruppe. *Neues Jahrb. Mineral., Abh.* **58**, 349-384.

Hassan, I. & Buseck, P.R. (1988): HRTEM characterization of scapolite solid solutions. *Am. Mineral.* **73**, 119-134.

Hawthorne, F.C. (1983): The crystal chemistry of the amphiboles. *Can. Mineral.* **21**, 173-480.

Hawthorne, F.C. (1994): Structural aspects of oxides and oxysalt crystals. *Acta Crystallogr.* **B50**, 481-510.

Hawthorne, F.C. (1997a): Short-range order in amphiboles: a bond-valence approach. *Can. Mineral.* **35**, 201-216.

Hawthorne, F.C. (1997b): Structural aspects of oxide and oxysalt minerals. *In* Modular Aspects of Minerals (S. Merlino, ed.). *Eur. Mineral. Union, Notes in Mineralogy* **1**, 373-429.

Hawthorne, F.C. (2002): The use of end-member charge arrangements in defining new mineral species and het-

erovalent substitutions in complex minerals. *Can. Mineral.* **40**, 699-710.

KULLERUD, K. & ERAMBERT, M. (1999): Cl-scapolite, Cl-amphiboles, and plagioclase equilibria in ductile shear zones at Nusfjord, Lofoten, Norway: implications for fluid compositional evolution during fluid–mineral interactions in the deep crust. *Geochim. Cosmochim. Acta* **63**, 3829-3844.

LIN, S.B. & BURLEY, B.J. (1973a): Crystal structure of a sodium and chlorine-rich scapolite. *Acta Crystallogr*. **B29**, 1272-1278.

LIN, S.B. & BURLEY, B.J. (1973b): The crystal structure of meionite. *Acta Crystallogr.* **B29**, 2024-2026.

LIN, S.B. & BURLEY, B.J. (1975): The crystal structure of an intermediate scapolite – wernerite. *Acta Crystallogr.* **B31**, 1806-1814.

MEIER, W.M. & VILLIGER, H. (1969): Die Methode der Abstandsverfeinerung zur Bestimmung der Atomkoordinaten idealisierter Geruestrukturen. *Z. Kristallogr.* **129**, 411-423.

OTERDOOM, W.H. & WENK, H.-R. (1983): Ordering and composition of scapolite: field observations and structural interpretations. *Contrib. Mineral. Petrol.* **83**, 330-341.

PAPIKE, J.J. & STEPHENSON, N.C. (1966): The crystal structure of mizzonite, a calcium- and carbonate-rich scapolite. *Am. Mineral*. **51**, 1014-1027.

PAPIKE, J.J. & ZOLTAI, T. (1965): The crystal structure of a marialite scapolite. *Am. Mineral.* **50**, 641-655.

PAULING, L. (1930): The structure of some sodium and calcium alumino-silicates. *Wash. Proc. Acad. Sci*. **16**, 453-459.

PETERSON, R.C., DONNAY, G. & LE PAGE, Y. (1979): Sulfate disorder in scapolite. *Can. Mineral.* **17**, 53-61.

PHAKEY, P.P. & GHOSE, S. (1972): Scapolite: observation of anti-phase domain structure. *Nature Phys. Sci*. **238**, 78-80.

REBBERT, C.R. & RICE, J.M. (1997): Scapolite–plagioclase exchange: Cl–CO_3 scapolite solution chemistry and implications for peristerite plagioclase. *Geochim. Cosmochim. Acta* **61**, 555-567.

SCHIEBOLD, E. & SEUMEL, G. (1932): Über die Kristallstruktur von Skapolith. *Z. Kristallogr*. **81**, 110-134.

SETO, Y., SHIMOBAYASHI, N., MIYAKE, A. & KITAMURA, M. (2004): Composition and $I4/m$–$P4_2/n$ phase transition in scapolite solid solutions. *Am. Mineral.* **89**, 257-265.

SHAW, D.M. (1960a): The geochemistry of scapolite. I. Previous work and general mineralogy. *J. Petrol.* **1**, 218-260.

SHAW, D.M. (1960b): The geochemistry of scapolite. II. Trace elements, petrology, and general geochemistry. *J. Petrol.* **1**, 261-285.

SHERRIFF, B.L., SOKOLOVA, E.V., KABALOV YU.K., JENKINS, D.M., KUNATH-FANDREI, G., GOETZ, S., JÄGER, C. & SCHNEIDER, J. (2000): Meionite: Rietveld structure-refinement, ^{29}Si MAS and ^{27}Al SATRAS NMR spectroscopy and comments on the marialite–meionite series. *Can. Mineral.* **38**, 1201-1213.

SHERRIFF, B.L.., SOKOLOVA, E.V., KABALOV YU.K., TEERTSTRA, D.K., KUNATH-FANDREI, G., GOETZ, S. & JÄGER, C. (1998): Intermediate scapolite: ^{29}Si MAS and ^{27}Al SATRAS NMR spectroscopy and Rietveld structure refinement. *Can. Mineral*. **36**, 1261-1279.

SOKOLOVA, E.V. & HAWTHORNE, F.C. (2008): The crystal chemistry of the scapolite-group minerals. I. Crystal structure and long-range order. *Can. Mineral.* **46**,

SOKOLOVA, E.V., KABALOV, YU.K., SHERRIFF, B.L., TEERTSTRA, D.K., JENKINS, D.M., KUNATH-FANDREI, G., GOETZ, S. & JÄGER, C. (1996): Marialite: Rietveld-structure refinement and ^{21}Si MAS and ^{27}Al satellite transition NMR spectroscopy. *Can. Mineral*. **34**, 1039-1050.

STOKES, H.T. & HATCH, D.M. (1988): *Isotropy Subgroups of the 230 Crystallographic Space Groups.* World Scientific Publishing, Singapore.

TEERTSTRA, D.K. & SHERRIFF, B.L. (1996): Scapolite cell parameter trends along the solid solution series. *Am. Mineral*. **81**, 169-180.

TEERTSTRA, D.K. & SHERRIFF, B.L. (1997): Substitutional mechanisms, compositional trends and the end-member formulae of scapolite. *Chem. Geol*. **136**, 233-260.

ULBRICH, H.H. (1973): Structural refinement of the Monte Somma scapolite, a 93% meionite. *Schweiz. Mineral. Petrogr. Mitt*. **53**, 385-393.

ZOLOTAREV, A.A. (1996): Once more on isomorphic schemes and isomorphic series in the scapolite group. *Zap. Vser. Mineral. Obshchest.* **125**(1), 69-73 (in Russ.).

ZOLOTAREV, A.A., PETROV, T.G. & MOSHKIN, S.V. (2003): Peculiarities of chemical compositions of the scapolite group minerals. *Zap. Vser. Mineral. Obshchest.* **132**(6), 63-84 (in Russ.).

Received December 6, 2006, revised manuscript accepted December 2, 2008.